THE SOFT X-RAY DIFFUSE BACKGROUND

D. McCAMMON, D. N. BURROWS, W. T. SANDERS, AND W. L. KRAUSHAAR

Department of Physics, University of Wisconsin, Madis

Received: _____

ABSTRACT

Maps of the diffuse X-ray background intensity covering essentially the entire sky with $\sim 7°$ spatial resolution are presented for seven energy bands: 130-188 eV (B band), 160-284 eV (C band), 440-930 eV (M_1 band), 600-1100 eV (M_2 band), 770-1500 eV (I band), 1100-2200 eV (J band), and 1800-6300 eV (2-6 keV band). The data were obtained on a series of ten sounding rocket flights conducted over a seven-year period. We have attempted to make the absolute intensities in these maps quantitatively accessible while still giving a clear qualitative display of the spatial features.

The different nature of the spatial distributions in different bands implies at least three distinct origins for the diffuse X-rays, none of which is well-understood. At energies $\gtrsim 2000$ eV, an isotropic and presumably extragalactic spectrum of uncertain origin dominates. Between 500 and 1000 eV, an origin which is at least partially galactic seems called for. At energies < 284 eV, the observed intensity is anticorrelated with neutral hydrogen column density, but we find it unlikely that this anticorrelation is simply due to absorption of an extragalactic or halo source.

Subject headings: X-rays: general -- interstellar: matter -- galaxies: Milky Way

Running title: SOFT X-RAY DIFFUSE BACKGROUND

I. INTRODUCTION

It has long been apparent that the soft X-ray diffuse background might provide unique information about the interstellar medium, the galactic halo, and hot intergalactic gas. However, the spatial distribution of the X-ray flux is complex, and one is easily misled in attempting to draw conclusions from trends observed in a limited area. Recognizing the need for a large data base, this group began in 1972 a program to map the distribution of the X-ray diffuse background over the entire sky as a function of energy in the 0.1 to 10 keV range. The survey was carried out on a series of ten sounding rocket flights with mechanically-collimated proportional counters having a 6 1/2° FWHM field of view. Both absorption-edge filters and pulse-height analysis were used to maximize the spectral information available.

The limited observing time on rocket flights places severe restrictions on the angular resolution that can be used and on the statistical precision of the results, especially when compared with what might be expected from a properly-designed satellite experiment. There are advantages with sounding rockets, however, that make these data complementary to existing and future satellite results on the diffuse background. Rocket altitudes are low enough ($\lesssim$ 200 km) to avoid much of the highly time-variable and often severe charged-particle background present at typical satellite altitudes (see for instance Bunner 1978). The rapid movement of a satellite through different geomagnetic regions further complicates the separation of diffuse X-ray data from extraneous background. A rocket experiment can be optimized for the single purpose of a diffuse sky survey, and instrument calibration can be checked both immediately before and shortly after the flight. We have taken advantage

of this latter capability to ensure that the absolute fluxes given here are as reliable as possible.

This sky survey has now been completed and all calibrations applied to the data. Analyses of some subsets of the data have been published previously (Williamson et al. 1974; Burstein et al. 1977; Sanders et al. 1977; Fried et al. 1980; Nousek et al. 1982). Extension of these detailed analyses to the full data set will be deferred to subsequent papers. The primary purpose of this paper is to make the complete set of survey data accessible for quantitative comparisons with models and other data.

The experiments and calibrations carried out are described in §II, and data-reduction procedures and energy-band definitions are outlined in §III. Section IV contains an extensive discussion of non-X-ray backgrounds and other sources of contamination. Maps of the counting rate in each of the energy bands are given in §V, which also includes a map of the neutral hydrogen distribution (Cleary, Heiles, and Haslam 1979) and conversions from counting rate to absolute fluxes for various spectral models. Brief discussions of the nature of the X-ray flux in the different energy bands are given in §VI. Since there is currently considerable observational and theoretical interest in a multi-phase galactic corona (Savage and de Boer 1981; Marshall 1981; Bregman 1982), the possibility that a hot component of such a corona could be the source of the observed X-rays in the lowest-energy bands is investigated in more detail at the end of this section. We conclude that while the X-rays are most probably thermal emission from a hot gas, the location and distribution of this gas are uncertain,

and there are grave difficulties with any simple model in which the observed intensity variations are caused only by absorption of flux from a galactic corona or any other source lying beyond most of the neutral hydrogen. In any case, barring the presence of an unsuspected solar system source that is both constant in time and very isotropic, at least the 1/4 keV X-rays seen in the galactic plane, which have an intensity almost one-third of the maximum observed in any direction, must originate within the galactic disk and no more than several hundred parsecs from the Sun.

II. THE EXPERIMENTS

a) Detectors

Observations were made using thin-window wire-wall proportional counters with three-sided anti-coincidence. The counters were filled with a 90% argon, 10% methane gas mixture at ∿ 1 atmosphere and were equipped with 2.5 cm thick 3mm-cell honeycomb collimators that gave a 5°5 FWHM circular field of view. Ceramic magnets were embedded in the collimator, providing a minimum field of 150 gauss throughout the honeycomb and extending 4 cm above it. The polarity was arranged so that electron trajectories which pass through the collimator without scattering at least once are intersected by the open experiment door for electron energies below ∿ 80 keV.

To ensure gain stability, the counter gas density was maintained at a constant value, and high voltage was furnished by very stable supplies. The counters were exposed to a ^{55}Fe 6 keV X-ray source every thirty seconds during the flights to provide gain calibrations. X-ray pulse heights were telemetered with a resolution of ∿ 2 eV from 30 eV to 1 keV, and with ∿ 20 eV resolution from 1 keV to 10 keV. The available energy resolution was therefore effectively that of the proportional counters themselves, with $E/\Delta E$ (FWHM) = 2.5 at 1 keV and varying as $E^{1/2}$. This is typical of good quality cylindrical proportional counters, but provides little energy discrimination

below 500 eV. To augment the spectral information in this range, boron and carbon K-edge filters were incorporated into the detector windows. On each flight, one counter had a 50 $\mu g\ cm^{-2}$ Formvar window coated with 200 $\mu g\ cm^{-2}$ of colloidal boron, while the second counter had a 270 $\mu g\ cm^{-2}$ polycarbonate window with a $\sim$ 10 $\mu g\ cm^{-2}$ colloidal carbon coating to provide electrical conductivity and reduce ultraviolet sensitivity. The thickness of this second window was chosen to minimize overlap with the boron bandpass while maintaining a usable transmission. For a more complete description of the windows, see Williamson and Maxson (1975). Open areas for the boror and carbon-filter counters were about 500 cm^2 and 800 cm^2, respectively. The boron area is smaller due to obscuration by the support mesh required for the thinner window. Two of the early flights were made with a payload containing somewhat smaller counters.

b) Calibrations

The transmission of the detector windows was measured before and after each flight at a number of X-ray energies. This was done on a grid of points over the entire window area, so that any non-uniformities in the thickness of the window or its coating could be accounted for.

Proportional counter non-linearities were measured at up to twenty-five energies before and after each flight. All sets of measurements for the series of flights were consistent with each other within their individual uncertainties, so all were averaged to produce the non-linearity curve used in the final analysis. Observed non-linearities

are due primarily to atomic effects at low energies and gain saturation at high energies. At an apparent gas gain of 1.5×10^4, saturation non-linearity was 15% at 6 keV. Atomic effects result in a discontinuity at the 248 eV argon L-edge of about 12%.

Counter gain variations were mapped over the entire detector surface. The maximum variation observed was < 10%, and the gain distribution was included in calculating the overall spectral response. Argon Kα escape characteristics were also measured, and the average effects of this process, which causes some events to be shifted down in energy by 3 keV and others to veto themselves, were used in the analysis.

A rough plastic coating was applied to the collimator surfaces to minimize X-ray reflections. Some reflectivity remains at low energies, and this was measured carefully at several wavelengths to obtain the true effective solid angle. The slightly larger FWHM beam shown on the maps for the two lowest energy bands is a result of these reflections. This is potentially the largest calibration uncertainty, but careful comparison of the laboratory measurements with models of the reflection lead to the conclusion that the adopted energy-dependent solid angles are within 10% of the true values (Burstein 1976).

As an in-flight test of our laboratory calibrations, we measured the spectrum and intensity of the Crab nebula on flight 13.122. The best-fit spectrum is $(9.3 \pm 0.4)\ E^{-(2.03 \pm 0.04)}$ photons $cm^{-2}\ s^{-1}\ keV^{-1}$ with absorption by $(2.6 \pm 0.2) \times 10^{21}$ H I cm^{-2} (1σ error bars) (Burrows 1982). The spectral fit had $\chi^2_{min} = 7.1$ for 6 degrees of freedom. This is in agreement with the results of Toor and Seward (1974).

c) Observations

Data were taken while scanning fan-shaped raster patterns, mostly at 5°.5 s^{-1}. Each flight covered about $\pi/2$ sr, or 1/8 of the sky. An inertial attitude control system with a typical absolute accuracy of 2° was used, and two 35 mm cameras allowed post-flight aspect determination to about 0°.2. A map showing the actual scan paths of all flights used in the survey is included in the Appendix, as is a table of physical parameters for each flight which lists the location, date, and time of launch, payload flown, and solar activity indices. All flights were made close to local solar midnight, and the bulk of the data were obtained at altitudes between 170 and 200 km.

III. DATA REDUCTION

a) Band Definitions

Keeping track of a complete pulse-height distribution for each point in a set of spatially-resolved data makes both display and analysis confusing. Since the energy resolution of the proportional counters is low for soft X-rays and the statistical precision for each spatial element is not great, little information is lost if the pulse-height spectra are integrated over a small number of discrete bins. Pulse-height limits defining the B and C bands were coordinated with the low-energy transmission characteristics of the boron- and carbon-filtered counters, respectively. High-energy bands combine data from both counters, with pulse-height limits chosen so that the band spacing reflects approximately the spectral resolution available from the proportional counters below 2 keV.

Figure 1 shows the product of net effective-area and solid-angle as a function of photon energy for each of the seven bands. This includes all the effects of window transmission, collimator reflections, proportional counter pulse-height distribution, non-linearities, gain variations, argon escape and self-veto, ob curation, and vignetting. The exact net counting rate in a band from any assumed X-ray intensity spectrum incident on the payload can be found by integrating the product of the spectrum and the band response curve. We should emphasize that

although the band responses have considerable overlap, the data in each band are statistically independent, since the counts come either from different detectors or from non-overlapping pulse-height intervals.

b) Normalizations

The response curves in Figure 1 apply directly only to flight 13.103. Small variations in window thickness cause the shapes of the curves to vary somewhat on different flights. In addition, the payload used on two early flights had counters with substantially smaller areas. In order to combine the data and to check for consistency in regions of overlap, it was necessary to derive normalization factors for other flights.

Laboratory calibrations were used to calculate a set of band response curves for each flight. Trial spectra were folded through these and the ratio of the predicted counting rate in each band to that predicted by the 13.103 response was calculated. Since the differences in shapes of the response curves were small and the range of models that had to be considered was highly constrained by the data, there was little uncertainty in these ratios. The careful derivation of these a priori normalizations enabled direct comparisons of the intensities measured by different flights in all overlap areas, and made possible the analysis of time-variable contamination discussed in §IV. For details of this derivation and analysis, see Burrows (1982).

c) Atmospheric Transmission

Model atmospheres were chosen according to the algorithm proposed by Jacchia (1972), in which solar and magnetic field activity indices, time of day, and geographical position are used to predict an exospheric temperature. Time of year and geomagnetic activity then give density corrections to be applied to the model for this temperature. In several cases where appropriate data were available, empirical fits to the atmospheric absorption were attempted using the uncorrected model atmospheres with exospheric temperature as a free parameter. In each of these cases, the best-fit model yielded a residual sum of squares no better than that of the model chosen and corrected by Jacchia's algorithm (Burrows 1982). Therefore we have employed this algorithm for each flight to chose a model for correcting the data for residual atmospheric absorption, using the photoelectric cross-sections of Henke (1967). Data for which the predicted atmospheric transmission was less than 80% were not included in the maps of §V.

d) Mapping Procedure

The desired map projection (Aitoff or polar equal-area) was divided into square pixels which are 1°.8 x 1°.8 at the center of the projection. Counts in each energy band were binned into 0.2 s intervals, during which the payload pointing direction moved at most 1°.1, and a deadtime-corrected cosmic ray background rate (see §IVa) was subtracted. The pointing direction was determined for the middle of each interval, and a conical approximation to the collimator response was used to weight all pixels within the field of view. The net counts were then divided up among the pixels according to these weights. The 0.2 s observing time,

corrected for electronic deadtime and atmospheric transmission, was similarly divided and stored in a second array. Counts and time maps were stored separately, and corrections applied to the time rather than the counts, so that maps could be combined and the approximate counting statistics recovered later. The counting rate maps in $V were produced by dividing the counts map by the exposure time map. A typical map of effective exposure time per pixel is included in the Appendix.

This mapping technique blurs the spatial resolution somewhat, and it is not self-consistent in the presence of features that are comparable in size to the collimation angle or smaller. It does, however, show a comforting resistance to the creation of false features, which is a problem with more sophisticated methods such as the algebraic reconstruction techniques when they are used on data sets with diffuse structure and limited statistical precision (Iwan 1978). One artifact which does appear in a few places on the maps is that a steep gradient at an oblique angle to the scan paths can be sharpened into a series of steps.

e) Point Source Removal

With the mapping technique described above, a uniformly-scanned point source would result in a count rate distribution that is the convolution of the actual collimator response and the conical approximation used in making the maps. This would have a FWHM of ~ 8.5 and a peak of half the actual peak counting rate, but the shapes are usually distorted somewhat by non-uniform coverage. In any case, counts will be dis-

tributed as far as the full width at base of the collimator response (16°) from the actual source position.

Strong discrete sources give much higher counting rates than the diffuse background, and they can distort the appearance of the background over areas much larger than the spatial resolution of the instrument. Since the primary purpose of this paper is to present data on the diffuse background, time intervals when one of the sources in Table 1 was within any part of the collimator field of view were eliminated before the maps were made. This does not affect the rates in the final maps except to eliminate any possible contribution from the discrete source and to reduce the exposure in the area surrounding it. Time intervals were eliminated without regard to whether the source could actually be seen in the data or not. The cut-off level for Uhuru sources was chosen to eliminate most of the ones which would otherwise have been noticeable in at least one of the energy bands.

IV. BACKGROUNDS AND CONTAMINATION

Extraneous signal sources are a serious potential problem in any measurement of a diffuse flux, since one cannot evaluate them directly by making nearby "off-source" measurements as is commonly done for observations of discrete objects. In the end, background levels can be estimated only by evaluating the behavior of each known candidate for interference and trying to place limits on its possible contribution.

Before discussing individual mechanisms, we can make some general observations which limit the likely magnitude of contamination problems. The first is that any source associated with the earth or solar system would most probably be variable in time, at least on the several-year time scale of this survey. Since many areas of the sky were observed on two or more of the rocket flights, we can test for any time-variable contamination. Second, a substantial fraction of the X-ray flux in the lower energy bands is in relatively sharp spatial features. For those which have been observed more than once, we can place upper limits of $\sim 5°$ on parallax and proper motion. The parallax limit implies distances $\gtrsim 20$ A.U., and any reasonable proper motion requires distances > 50 A.U. This guarantees that the part of the flux contained in many of the features originates no closer than the outer parts of the solar system. However, the minimum observed X-ray flux is more than one-third of the average flux for each of the energy bands, and there is no way to rule out an unrecognized local source at this level which is both isotropic and constant in time.

a) Non-X-ray Backgrounds

The most obvious background is response to cosmic rays, which we define to be high-energy nuclei, gamma rays, and other radiations that can easily penetrate the entire payload and for which the detector pointing direction is therefore generally immaterial. These events typically deposit amounts of energy in the counters which are in the same range as the X-ray energies of interest, and their fluxes ($\sim 1\ cm^{-2}\ s^{-1}$) are much higher than observed X-ray rates. The surrounding anti-coincidence counters discriminate quite efficiently against cosmic ray events, but charged particle trajectories crossing the small unprotected ends of the counters and Compton interactions in the gas produce a small residual counting rate. This rate can be evaluated both when the payload door is shut and when it is open with the detectors pointed toward the earth. The rates are observed to be the same in both cases, and to be independent of altitude above 60 km and constant from one flight to the next. The cosmic ray rates in each energy band range from 3% of the average X-ray rate in the C band to 12% in the 2-6 keV band, and have been subtracted from the data presented in these maps.

Ultraviolet photons from stars can liberate photoelectrons from ground-plane wires and the inner surface of the window. These electrons initiate avalanches with a mean pulse-height equivalent to $\sim$ 30 eV, but the distribution of pulse-heights is approximately

exponential and a significant fraction will be at amplitudes used in the X-ray analysis. The boron filter is very opaque to UV and no problems are expected with this counter. The polycarbonate window used for the carbon filter cuts off at 2400 Å, and was coated with an additional 10 $\mu g\ cm^{-2}$ of colloidal graphite to suppress transmission at longer wavelengths. Laboratory tests on the windows predicted no response to UV levels expected in flight, and no bright stars were detected during any of the observations. As an additional check, pulse-height spectra were routinely examined; falling window transmission at low energies causes predicted pulse-height spectra to drop off toward the lower discriminator for all X-ray spectra otherwise consistent with the data, while the pulse-height distribution from UV would rise steeply. A drop-off, which limits any possible ultraviolet contribution to a very small fraction of the observed rate, was always observed. (For typical pulse-height spectra, see Fried et al. 1980.)

Electrons in the 2-50 keV range can penetrate the counter windows and stop in the front gas volume without entering the surrounding anti-coincidence layers. At the low end of this range, their residual energies after passing through the window can be in the 0.1-10 keV interval, and such events are individually indistinguishable from X-rays of the same energy. The magnets described in §II are not completely effective in eliminating this kind of background, since electrons which scatter one or more times can still enter the detectors.

A sensitive test for the presence of such events is to look at the apparent flux in the 2-10 keV range. At these energies the diffuse X-ray background is nearly isotropic and we have used detectors with a front anticoincidence layer to determine its uncontaminated intensity. The pulse-height distribution predicted from this spectrum for the front layer or for a single-layer counter can be compared with the observed distribution, and any difference attributed to electrons. Since the electrons lose at least 2 keV in the windows, their apparent spectrum inside the counter is quite flat at low energies, and a conservative extrapolation of the electron spectrum determined in the 2-10 keV region will generally give an upper limit at lower energies that is a small fraction of the steeply-rising X-ray spectrum, even when the electron contamination is relatively large at 6 keV. This procedure is described in more detail by McCammon (1971). Such an examination of the data for the ten flights in the survey shows definite evidence for electrons in only one, where there is an excess of 12% in the 2-6 keV band. An extrapolation to the lower bands indicates a 3% contribution to M bands, 1% to C band, and 3% to the B band. This flight was 13.137, which also had the highest geomagnetic activity index during the previous week, but one of the lowest for the 24 hours preceeding the launch.

b) Extraneous X-rays

What is "extraneous" depends on how one intends to interpret the results, but for current purposes it seems reasonable to wish to exclude any emission associated with the solar system. We proceed to discuss potential mechanisms for the production of X-rays within the solar system, and then describe an observed time-variable X-ray contribution to the B and C bands which is probably associated with one or more of these.

The solar wind carries enough energy to produce all of the B and C band X-rays if it were converted entirely to photons of the appropriate wavelengths at a distance of less than $\sim$ 600 A.U., and the streaming velocity of the protons is equivalent to a much higher temperature than would be required. Predicted postshock temperatures at thermalization are near the required 10^6 K, but the calculated densities are so low that pathlengths of tens of parsecs would be required to produce an appreciable X-ray flux (Axford 1972; Yu 1974). Random velocities within the solar wind approach the X-ray emitting range, but calculations by José Franco of this laboratory indicate that both temperatures and densities are too low to have a significant effect. Still, these must remain as unlikely but nagging possibilities.

Solar X-rays scattered by the Earth's atmosphere were observed on several early soft X-ray experiments (Hayakawa et al. 1970; Grader et al. 1970). Calculations by Hayakawa et al. (1971) are in quite reasonable agreement with these observations. Flights in this survey were made as close to local solar midnight as possible, and the solar zenith angle was 125° on two of the flights and exceeded 130° for all the rest. The

calculations of Hayakawa et al. predict an entirely negligible contribution from this source for all of the flights.

It has long been recognized that electrons precipitating into the atmosphere can produce intense bremsstrahlung and fluorescent X-rays in auroral zones, and more recently X-rays attributed to this mechanism have been observed at low latitudes (Luhmann et al. 1979). Low-energy electron fluxes are highly variable in time and very dependent on geographical location and altitude. The distribution of these fluxes in both time and space is too uncertain to predict the probability of significant X-ray from this mechanism during our rocket flights.

If similar electrons penetrate as low as 200 km, they can produce bremsstrahlung and fluorescent X-rays directly from surfaces of the payload. The electron spectrum must be quite steep, or the much more efficient direct detection of electrons above 2 keV which can penetrate the window would dominate these soft X-rays. Again, the variability in electron fluxes and scarcity of data at low altitudes precludes a prediction of the potential size of this effect.

To test for the presence of any contamination which varied over the seven years of the survey, the normalizations discussed in §IIIb were applied and the data examined for differences wherever two flights overlapped. Among the ten flights there were twenty-five pairs with usable overlaps. Analysis of these twenty-five differences indicates that five of the flights show little or no evidence for contamination. The other five show contamination which was typically 30 cts s^{-1} in the C band and 10 cts s^{-1} in the B band, and which was observed to be as high as 70 cts s^{-1} and 33 cts s^{-1} respectively in these bands. There is also some evidence for a much smaller amount of contamination in the M bands.

The spatial distribution of this contamination was anisotropic on some of the flights. On two of these it shows an increase toward the northern horizon, but on others it does not. On some it appears patchy. There is no detected correlation with ecliptic coordinates or altitude, and very little with zenith angle or angle to the Earth's magnetic field. The contamination rate from a fixed point in the sky was never observed to vary during a single flight, but it changed substantially between two flights that were twelve days apart. This fixes the time scale for the variations as somewhere between minutes and weeks.

Two of the overlap regions contained enough counts to derive good pulse-height spectra of the contamination. These spectra are not identical, but both appear to be caused by a broad soft X-ray spectrum not too different from that of the diffuse background below 284 eV.

The most likely candidates for the source of this contamination seem to be either the "auroral" X-rays discussed above or bremsstrahlung from low-energy electrons on the payload itself. In either case, the electron spectrum must be very steep. For auroral X-rays, it can be shown that a power-law index greater than 2.8 is required to prevent oxygen Kα fluorescence, which would show up in the M band, from dominating the low-energy bremsstrahlung (Kraushaar 1974, Williamson 1974). For X-ray production at the payload, carbon Kα fluorescence overwhelms bremsstrahlung for electron energies above 300 eV, and a pure C Kα line would be inconsistent with the observed pulse-height spectra. The lack of altitude dependence (from 150 to 200 km) would be surprising

for soft electrons at the payload, as would the very small correlation with angle to the B-field, although this latter relation could certainly be confused by the detector magnets. On the other hand, auroral X-rays would be expected to show a much stronger concentration toward the northern horizon than was observed. Also, an unexpected background observed on flights of a Bragg crystal spectrometer had a pulse-height distribution virtually identical to this contamination and was consistent only with a source local to the payload.

For either of these mechanisms, one would expect a correlation with geomagnetic activity, since measured electron fluxes generally show such a correlation. In fact, the two flights with the largest contamination have the largest K_p indices at launch, but the third-largest contamination was observed on the flight with the lowest K_p of all ten. Perhaps more than one source mechanism contributes to the observed flux.

The lack of a consistent pattern to the spatial distribution makes it difficult to extrapolate contamination levels to areas where they cannot be determined directly. Data from contaminated flights were eliminated from the maps wherever there was uncontaminated coverage of the same area, but suspect data were left in if there was no better coverage of that part of the sky. Suspect areas and our best estimate of the rates in the B and C bands from contamination in those areas are shown in Figure 2. These estimates are in reasonable agreement with contamination rates derived from a comparison of our C band map with similar data from the SAS-3 experiment (Marshall 1982a).

c) Summary

Except for a 12% contribution to the 2-6 keV band on one flight from electrons penetrating the detector windows, there is no evidence for significant non-X-ray contamination of the data. There appears to be a more severe extraneous X-ray contamination which affects the B and C bands on portions of half the flights. Estimates of the counting rate contribution of this spurious source to various parts of the B and C band maps are shown in Figure 2.

V. MAPS

Figures 3-9 show maps of the diffuse X-ray counting rates in each of seven energy bands. Energy limits at the 20% response points are given in the respective captions. The all-sky map in each figure is an Aitoff equal-area projection centered on $\ell = 0°$. In this projection, the small square pixels are 1°.8 x 1°.8 at the center of the maps, and represent a solid angle of exactly $(1°.8)^2$ at any position. This has the advantage that relative areas of features are always correctly displayed. Shapes are highly distorted near the edges, however, so for each of the five lower-energy bands we have included three partial projections which give more optimum presentations for those parts of the sky. The three are an Aitoff centered on $\ell = 180°$ and two polar equal-area projections for the regions around the north and south galactic poles. Pixels on these projections are also $(1°.8)^2$, and all maps are reproduced at the same scale.

The change in counting rate for each shading step is given in the figure captions. There is no offset and 0 cts s^{-1} would be no shading, but in fact observed counting rates were almost never less than one-half a shading step, and unshaded areas generally indicate no coverage. The contour interval is half of the shading interval on all maps, so every contour is unambiguously labelled by the pixel shading. For example, the C band map has a shading interval of 40 cts s^{-1}. A contour which has pixels containing three vertical bars on both sides of it is at the

third shading level, which is 120 cts s^{-1}. A co. tour which separates pixels with three bars from pixels with four bars is halfway between the third and fourth shading levels, or 140 cts s^{-1}.

A standard set of bright discrete sources has been removed from the maps for reasons discussed in §IIIe. Some remaining features that can be attributed at least in part to identifiable discrete sources are listed in Table 2. With the exception of the two supernova remnants, these show up only in the higher-energy bands.

Neutral hydrogen column density data from Cleary, Heiles, and Haslam (1979) is shown in Figure 10 on the same projection as the X-ray maps. In this figure, the shading interval is 1.0×10^{20} H I cm^{-2}, and the contour levels are 0.5, 1.5, 2.5, etc., $\times 10^{20}$ H I cm^{-2}.

The absolute counting rate in a band from any assumed spectrum can be found by integrating the product of the spectrum and the band response curve given in Figure 1. This has been done for several simple spectra, and the results are given in Table 3 along with some other characteristics of each band. Figure 11 shows the predicted counting rate per unit emission measure as a function of temperature for radiation from a hot plasma with solar abundances in thermal equilibrium (Raymond and Smith 1979). The assumption of thermal equilibrium in interstellar plasmas is questionable (Hayakawa et al. 1979a), but these spectra have become a convenient standard for comparing observations. Figure 11f gives the total energy flux integrated from 10 to 5000 eV per unit emission measure as a function of temperature for these same spectra.

VI. DISCUSSION

Several detailed analyses of subsets of the data from this survey have been published previously. Burstein et al. (1977) discussed fitting of thermal emission spectra, Sanders et al. (1977) and Fried et al. (1980) proposed models for the low-energy (B and C) bands, and Nousek et al. (1982) analyzed possible models for the intermediate-energy (M_1, M_2, and I) bands. Although there is considerable additional information in the full data set, we see nothing that directly contradicts any of the conclusions reached in these studies. We will defer more extensive analysis of the data to future papers, and limit this section to pointing out the general characteristics of the X-ray background as one looks at it in the different energies covered by this survey.

A cursory examination of the maps shows that the nature of the spatial distribution changes dramatically between the 2-6 keV band and the M_1 and M_2 bands, and again between the M bands and the B and C bands. The J and I bands are a transition region, with the J band looking more like the 2-6 keV band and the I band resembling the M_1 and M_2 bands. In contrast, the transition is quite sharp between the M_1 band and the C band, at least in part because the carbon contained in all the detector windows produces a gap in the energy response between 284 and $\sim$450 eV.

The possible nature of the X-ray emission in each of these three regions is outlined below. In the case of the B and C bands, the most straightforward conclusions that can be reached from the qualitative appearance of the data seem to be contradicted by a quantitative analysis. We therefore include a more extensive discussion of this problem.

a) 2-6 keV Band

The 2-6 keV band is really the low end of the high-energy X-ray diffuse background. The Galaxy is still almost entirely transparent, and the observed flux is highly isotropic and believed to be predominantly extragalactic. More sensitive surveys than ours in this energy region have revealed two anisotropic galactic components at low flux levels (Warwick, Pye, and Fabian 1980; Worrall et al. 1982; Iwan et al. 1982). The origin of the major cosmological component of the flux is unknown, but there are several known or suspected contributors. For a recent review, see Boldt (1981).

In the 2-6 keV range, the spectrum is well-fit by an 11 $E^{-1.4}$ photons cm^{-2} s^{-1} keV^{-1} power-law on all flights where it is uncontaminated by electrons (see §IVa), although it becomes progressively steeper at higher energies. It is usually assumed that this spectrum can be extrapolated below 2 keV, but there is really no evidence for its existence anywhere below $\sim$ 1.5 keV. There is also no good evidence that it turns over (see however Bunner, Sanders, and Nousek 1979, and Seward and Mitchell 1981), although its extrapolation to the 0.5-1. keV region causes some difficulties which are pointed out in

§VI b below. The existence and location of any such turnover would provide a valuable clue about the origin of this spectrum, but confusion by local emission makes such a determination difficult.

b) M_1 and M_2 Bands

Structure in the M bands is dominated by a blotchy irregular feature about 110° in diameter located in the general direction of the galactic center. Its boundaries coincide roughly with the outline of radio Loop I (Berkhuijsen, Haslam, and Salter 1971), extending somewhat beyond it in the southern galactic hemisphere where Loop I itself is not well-defined by any bright radio continuum ridges. The two brightest areas in the northern half line up very well with the inner edges of the brightest radio ridges defining the Loop, and there can be little doubt that they are related. It is therefore tempting to associate this entire X-ray feature with the interior of Loop I. The nature of this interesting object and its connection with X-ray emission have been discussed by Borken and Iwan (1977), Hayakawa et al. (1979b), Davelaar, Bleeker, and Deerenberg (1980), Iwan (1980), Heiles et al. (1980), and Nousek et al. (1982).

Two other, much smaller, features that can be distinguished on these maps are the Eridanus-Orion enhancement near 200°,-35° (Naranan et al. 1976; Reynolds and Ogden 1979; Nousek et al. 1982), and the Cygnus "superbubble" at ∿ 80°,+5° (Cash et al. 1980). All three of these

objects have been proposed to be large cavities in the interstellar medium, formed either by stellar winds from young associations or by a series of supernovae, and then heated at a large diameter by a subsequent supernova.

Aside from those features the M band maps have very little structure. They are somewhat patchier than expected from counting statistics, but show almost no systematic pole-to-plane variation. This is quite surprising, since photon mean free paths in these bands are about a kiloparsec: a scale length on which the interstellar medium is quite anisotropic. If the 11 $E^{-1.4}$ spectrum observed in the 2-6 keV band is extrapolated to the M bands, it will provide about 55% of the flux seen at the poles. This drops to 30% at $\sim$ 10° latitude and to zero in the plane due to interstellar absorption. Rosner et al. (1981) have investigated the X-ray luminosities of various stellar types and find that dM stars could contribute as much as 25% of the flux in these bands. This would provide a component which increases toward low latitudes to help fill in the absorption of the extra-galactic spectrum, but since the scale-height of the stars is higher than that for the absorbing gas, there would still be a dip in the plane.

It has been shown that if a model is constructed which combines these two components with a population of objects like the super-bubbles discussed above, plus a contribution from whatever is making the flux observed in the B and C bands, then by carefully

adjusting the relative contributions it can be made to have almost no bump or dip at the plane (Sanders et al. 1982). The parameters for each component in this model all come out with very reasonable values; most are even what one would have picked ahead of time. Still, it is not very satisfactory to require such an exacting balance among so many components, each with a large latitude variation, in order to reproduce an observation with almost no latitude dependence. We continue to regard the source of most of the M band flux as an unsolved problem.

c) B and C Bands

The spatial distribution in the B and C bands is quite different from that in the M bands. Both of the lower energy maps show a general increase in count rate toward the galactic poles, particularly in the northern hemisphere. Comparison with the N_H map shows a striking anticorrelation between X-ray intensity and H I column density. That this is more than just their opposite latitude dependence is graphically illustrated in Figure 12, which shows how the correlation between the C band map and the N_H map varies as the N_H distribution is rotated around the galactic polar axis. The sharp peak at 0° indicates a real anticorrelation of longitudinal structure on the two maps, while the high residual anticorrelation at all rotation angles is caused in part by the general latitude variations.

Diffuse thermal emission seems to be the most likely source of these X-rays. If discrete sources in the galactic disk provided the majority of the observed flux, limits on small-scale fluctuations would require a space density at least equal to that of the most common stars (Levine et al. 1977). Stars themselves provide at most 2-3% of the flux (Rosner et al. 1981), so a truly diffuse source seems to be required. All non-thermal diffuse mechanisms which have been considered seem easy to rule out (Williamson et al. 1974), and the power law spectrum observed above 2 keV would provide less than 20% of the maximum observed intensity even if one discounts absorption. This leaves diffuse thermal emission from gas at $\sim 10^6$ K as the probable source. The existence of such gas was suggested long ago (Spitzer 1956), and observations of interstellar O VI (Jenkins and Meloy 1974; Jenkins 1978a,b) now provide solid evidence for the existence of gas at only slightly lower temperatures.

If the material producing the X-rays were located beyond the galactic neutral gas, then absorption by this cool interstellar material would provide a natural explanation for the observed anticorrelation of X-ray intensity and neutral hydrogen column density. While a truly extragalactic origin for the B and C band X-rays seems unlikely due to lack of apparent absorption in extragalactic objects (McCammon et al. 1971, 1976; Long, Agrawal, and Garmire 1976), a hot galactic halo or corona has a sound

theoretical basis (Spitzer 1956; Chevalier and Oegerle 1979) and there is observational evidence for the existence of highly ionized material far above the plane (Savage and de Boer 1981). Radiation from hot gas in a galactic corona is therefore an attractive possibility.

There are, however, problems with the model of an absorbed coronal origin for the B and C band X-rays. We have examined the general X-ray intensity vs. H I column density relation to quantitatively test this model as an explanation of the anti-correlation of B and C band intensities with N_H. Five major difficulties are apparent:

1) In spite of the very short mean free path, there is residual flux in the galactic plane which is about 30% of the observed maximum intensity. This problem is resolved by including in the model an isotropic local (unabsorbed) X-ray emission component.

2) There is more scatter in the H I column density vs. X-ray intensity relation than is consistent with a simple absorption model. The problem may be with the H I data, since the radio beam side-lobe contributions to the 21 cm column densities can amount to a large fraction of an optical depth at these X-ray energies (Heiles, Stark, and Kulkarni 1981). Another possibility is that the local X-ray component is not isotropic.

3) The experiments of McCammon et al. (1971, 1976), and Long, Agrawal, and Garmire (1976), designed to test with high statistical precision for X-ray absorption by the Magellanic clouds, also detected no absorption by galactic gas. Two independent 21 cm surveys were used to analyze the data of McCammon et al. and gave very similar limits, so inaccuracies in the H I data seem an unlikely explanation for the negative result.

4) Quantitatively, the X-ray intensity variations with changing column density are much smaller than predicted by the atomic absorption cross-sections of Brown and Gould (1970).

5) The X-ray intensity variations do not show the large energy-dependence predicted by photoelectric absorption. The calculated cross-sections for the B and C bands differ by a factor of 2 (1.7×10^{-20} cm^2 and 0.8×10^{-20} cm^2, respectively), whereas the observed effective cross-sections required for consistency with the absorption model are almost identical (0.40×10^{-20} cm^2 for B band and 0.37×10^{-20} cm^2 for C band).

A natural explanation for the anomalous absorption behavior is clumping of the absorbing gas. As pointed out by Bowyer and Field (1969) and Bunner et al. (1969), if the interstellar gas were clumped on angular scales smaller than the X-ray beam into randomly-distributed clouds of thickness N_{cl}, then the effective X-ray cross-section, σ_{eff}, would be

$$\sigma_{eff} = \frac{1 - e^{-\sigma N_{cl}}}{N_{cl}} \qquad (1)$$

where σ is the Brown and Gould (1970) X-ray absorption cross-section per atom of interstellar material. Thus, clumping with $N_{cl} \sim 2.4 \times 10^{20}$ cm^{-2} will reduce the B band cross-section to 0.41×10^{-20} cm^2 and the C band cross-section to 0.36×10^{-20} cm^2, in good agreement with the observations. Bunner et al. (1969) and Marshall (1982b) have found just slightly larger values of N_{cl} to be required for fits to similar two-component models, and the results of Davidsen et al. (1972) are also consistent. It appears, then, that having almost all interstellar material in clouds of $2\text{-}3 \times 10^{20}$ cm^{-2} average thickness would resolve the most serious difficulties with the otherwise attractive coronal model.

However, observational evidence is lacking for such cloud structure in the interstellar gas at intermediate and high galactic latitudes, and existing 21 cm observations place severe constraints on the angular scales of clumping at this level. The Hat Creek 21 cm survey (Heiles 1974) has an angular resolution of $\sim 36'$. Averaging the transmission of all H I column density measurements within a 7° diameter X-ray field of view and comparing it with the transmission of the averaged column density gives N_{cl} from equation (1) which is typically only 0.15×10^{20} cm^{-2}. A similar test on some data taken by Verschuur (1974) at intermediate latitudes gave almost identical results for an effective angular resolution of 10'x20'. Therefore almost all of the required structure would have to be on angular scales smaller than 36'. At high galactic latitudes this implies small linear dimensions and high densities.

Interferometric 21 cm absorption studies and emission measurements using the 3' beam of the Arecibo telescope seem to rule out significant amounts of structure on angular scales from arc seconds up to twenty arc minutes at intermediate and high galactic latitudes (Greisen 1976; Dickey 1977, 1979; Dickey and Terzian 1978; Dickey, Salpeter, and Terzian 1979; Payne, Salpeter, and Terzian 1982). In addition, Dickey, Salpeter, and Terzian (1979) find that $\sim$ 78% of the total column density at high latitudes appears as "not strongly absorbing" material, with lower limits on spin temperature from 300 K to 1000 K. Such material is commonly (Clark 1965; Radakrishnan 1974), but not universally (McKee and Ostriker 1977), ascribed to a structureless warm intercloud medium. If this material is really structureless, no amount of clumping of the remaining gas would be sufficient to reduce the effective cross-section to the necessary value.

Finally, interstellar UV absorption measurements also are difficult to reconcile with such thick clouds. Bohlin, Savage, and Drake (1978) have used the Copernicus satellite to determine molecular and atomic hydrogen column densities to five stars with $|b| > 20°$ and distances between 100 and 1000 pc. All of these stars show total column densities between 0.7 and 1.8×10^{20} cm^{-2}. If this gas were really in clouds of more than 2×10^{20} cm^{-2} thickness, we would expect fluctuations on the order of 100%, even assuming that the spatially-smoothed column densities out to the distances of these widely-spaced stars are all equal. Instead, the measured mean and standard deviation, $1.32 \pm 0.43 \times 10^{20}$ cm^{-2}, formally imply clouds less than 2×10^{19} cm^{-2} thick.

The UV absorption sample is very small, and we do not think that an airtight case against clumping on all angular scales can be made at the present time from the radio data. However, it is certainly true that any model which requires that almost all of the interstellar material at intermediate and high galactic latitudes be in 2×10^{20} cm^{-2} clouds must be squeezed rather awkwardly into current observational limits.

An empirical test of interstellar X-ray absorption can be made by looking at objects whose intervening column densities are known. Investigations of soft X-ray absorption in the spectra of nearby supernova remnants, where there is no real possibility of self-absorption in the source, are entirely consistent with standard atomic cross-sections (Ryter, Cesarsky, and Audouze 1975; Ride and Walker 1977). Looking for evidence of interstellar absorption in our own data, the Cygnus Loop is the brightest source in the C band, while the Vela supernova remnant, with less foreground gas, is brighter in the B band (The intrinsic B to C ratios are rather insensitive to temperature in the relevant range). Energy-dependent absorption can also be seen in the Loop I X-ray features, where a well-defined sheet of neutral hydrogen extends northward from the plane in front of Loop I. The X-ray spurs extending down just inside longitudes 30° and 290° show up in all bands from B to I, and they can be seen to fade out further and further from the plane as one goes to the lower-energy bands. Quantitative estimates of the X-ray absorption by Morrison (1979) are consistent with other

measures of the intervening gas. These observations of the expected strong energy-dependence argue against the energy-independent absorption required by the two-component model.

Another way of producing the observed anti-correlation has been suggested by Sanders et al. (1977) and Fried et al. (1980), who propose that since a local emission component seems required in any case, it could provide essentially all the observed flux in the B and C bands. Assuming that the source is thermal radiation from a diffuse plasma, the required temperature is near 10^6 K. Pressure arguments then favor an extent of roughly 100 pc, in good agreement with optical interstellar absorption results, which show a region of anomalously low density of similar extent around the sun (Cash, Bowyer, and Lampton 1979; Bruhweiler and Kondo 1982, and references therein). This is comparable to the scale height of the H I distribution, so the hot material displaces a significant column density of neutral gas. If spatial features in the B and C bands are caused by variations in the extent of the emitting region, we would expect them to be anticorrelated with H I column density due to corresponding variations in the amount of neutral gas displaced. Unfortunately, this displacement model makes few quantitative predictions that can be tested without knowing the three-dimensional distribution of cool interstellar material in the solar neighborhood. One definite prediction which agrees well with observations is that

the correlation with H I should be entirely energy-independent, but this was one of the major factors which inspired the model in the first place.

A potentially useful test is to check for any correlation with high velocity neutral hydrogen. Since there is very little material with $|v| > 20$ km s^{-1} in the vicinity of the Sun, any correlation with this gas component would argue strongly against the displacement model. Correlations caused by absorption should of course persist. We have carried out a correlation analysis with the above test in mind and find the high velocity gas to be uncorrelated with C band X-rays. Taken at face value, this test would appear to rule out any model in which a substantial fraction of the flux originates beyond the high velocity gas. However, the brightness temperatures of high velocity 21 cm profiles at high galactic latitudes are small, side-lobe contributions can be important, and we feel that this type of test can be definitive only when better quality 21 cm data are available.

While we find the paucity of detailed predictions of the displacement model unsatisfying, the straightforward quantitative predictions of simple two-component models with two isotropic components in which one component lies beyond the neutral gas seem very difficult to reconcile with what is known about the interstellar gas distribution. If an extragalactic or coronal source provides a substantial fraction of the observed low-energy X-rays, some model of the interstellar medium other than simple clumping of the cool material will be required.

It might also be that the local component has a simple spatial structure and that absorption of a halo source could then provide the detailed anticorrelation with interstellar gas with more nearly the expected atomic cross sections. The analysis of such models is a complex problem and will be considered in a separate paper.

Avenues of investigation which would help determine the location of the very soft X-ray emission include comparisons of the X-ray data with more reliable 21 cm column density measurements, and some additional 21 cm observations to put limits on clumping in the several arc minute to one degree range which is now only weakly covered. Extension of the X-ray observations to longer wavelengths would also be very helpful: if the similarity in spatial distribution seen in the C and B bands persist at lower energies, it will be a stronger argument in favor of a local origin for all of these X-rays. Measurements at such wavelengths by Levine et al. (1977) and Stern and Bowyer (1979) show a large flux, but have insufficient coverage to determine the spatial distribution.

VII. CONCLUSIONS

Maps of the X-ray diffuse background have been presented for the 0.1 - 6 keV energy range. Every effort has been made through careful calibrations and cross-checking to minimize known sources of systematic error and test for unexpected ones. Except as noted above, we think that 15% is a reasonable upper bound to residual systematic effects. The most important exception is in the B and C bands, where 25% of the sky may be contaminated to a significant extent by extraneous X-rays as indicated in Figure 2.

The changing character of the observed spatial distribution with energy and the rapidly varying interstellar mean free path appear to separate the 0.1 - 6 keV range into three energy regions where qualitatively distinct components must dominate the diffuse background: 1) above 2 keV, the extragalactic high energy background predominates; 2) between 0.5 and 1.0 keV, the X-ray flux is nearly isotropic, with a few identifiable extended features superposed; and 3) below 0.28 keV the flux increases markedly and is highly anisotropic, with intensity variations of more than a factor of three from one part of the sky to another which are generally anticorrelated with variations in H I column density.

In each of these regions, the predominant diffuse background component shares two characteristics: it strongly dominates flux from identifiable discrete sources, and it is not well understood. For E > 2 keV, more detailed data are available elsewhere (Schwartz *et al.* 1979; Marshall *et al.* 1980).

In the 0.5 - 1.0 keV range, the interstellar mean free path is on the order of 1 kpc, and sources on a galactic or more distant scale should show strong anisotropies. The observed isotropy is therefore most naturally explained by assuming a local source, but one must then reduce contributions from the high energy diffuse spectrum and integrated dM-star luminosity below their expected levels. It is also possible to construct models which include these contributions and balance various components to approximately cancel the galactic latitude dependences.

Below 0.28 keV, the rather detailed anticorrelation with H I strongly suggests absorption of an extragalactic source. However, quantitative analysis shows that it is very difficult to reconcile simple models of this sort with existing 21 cm observations: the smaller-than-expected absorption and lack of energy dependence seem to require that all of the interstellar gas be clumped to an extent that is virtually ruled out by the radio data. Some other explanation of the anomalous absorption cross sections would be required. Displacement of neutral hydrogen by variations in the extent of a local region filled with hot X-ray emitting gas could also produce the observed anticorrelation and would automatically have the necessary energy-independence. There are no definite arguments against having this local emission region provide all of the observed flux, but it seems likely that neither of these simple models is entirely correct.
The low-energy X-rays are most probably thermal radiation from gas at

about 10^6 K, but the location of the observed emission and the larger question of the pervasiveness of such material and its implications for the nature of the interstellar medium are still observationally undetermined. Improved neutral hydrogen column density data, some information on its three-dimensional distribution in the vicinity of the Sun, and additional X-ray data at lower energies or with higher spatial resolution should all contribute greatly to understanding this interesting component of the diffuse X-ray background.

This research was supported by the National Aeronautics and Space Administration under grant NGL 50-002-044. A project of this duration has naturally involved the efforts of many. We gratefully acknowledge the contributions of: R. J. Borken, A. N. Bunner, P. Burstein, W. Cartwright, P. L. Coleman, E. Conrad, B. Eltman, H. Ferguson, P. M. Fried, J. Hoessel, S. Holz, D. Hutchins, S. Iltis, D. C. Iwan, C. M. Jaehnig, P. LaMaster, J. Lenz, C. Maxson, S. S. Meyer, W. Moore, J. Morrison, R. Morrison, J. A. Nousek, J. Peters, D. Pfrang, T. Quigley, R. Riese, M. P. Ulmer, M. J. Vanderhill, and F. O. Williamson. We thank Don Cox for his consistent encouragement and Fred Marshall for sharing his SAS-3 map prior to publication. The personal and highly professional assistance of many individuals at the Sounding Rocket Division of Goddard Space Flight Center and the Aerobee launch crew at White Sands missile range is deeply appreciated.

APPENDIX

INDIVIDUAL FLIGHT PARAMETERS

Table 4 lists basic information about each of the ten sounding-rocket flights making up the all-sky survey. Two different payloads were employed. Payload IV, used on all but two of the flights, had a carbon-filter counter with 830 cm^2 net open area, and a boron-filter counter with 475 cm^2 open area. Both of these detectors had 2.5 cm-thick active layers with anticoincidence counters on three sides separated by fine wire walls. Payload III, used on two of the early flights, contained smaller counters with 460 cm^2 net area for the carbon filter and 260 cm^2 for the boron filter. These counters had a 1.8 cm-thick front layer and a 5.9 cm-thick back active layer in addition to the three-sided anticoincidence. This multi-layer construction was used to test for electron contamination and to make other consistency checks on derived spectra. All counters were filled with a 90% argon, 10% methane mixture at a density corresponding to 780 torr at 20 °C for White Sands launches and 860 torr at 20 °C for flights from Woomera. Table 5 gives the proportional counter pulse-height limits used to define each of the bands and the energies where the net response falls to 20% of maximum for the band. Data for the B and C bands come only from the detector with the corresponding filter, while data from both detectors are combined for the higher-energy bands.

Figure 13 shows the scan paths for all ten flights. Most scans were made at about 5°.5 s^{-1}. The path for flight 25.045, which had a malfunctioning attitude control system, is shown as a dashed line. Scan rates were generally rather high on this flight ($\sim$12° s^{-1}), so it contributed little data to the maps, but it did provide a number of useful cross-checks. B and C band data from 25.045 were not used in the maps.

Figure 14 is an exposure-time map for the C band. The exposure time for a 1°.8 x 1°.8 pixel with N shading bars is $10^{N/2}$ milliseconds. As on the count-rate maps, there are two contours per shading interval, so the contour interval is 0.25 in $\log_{10}$ (exposure time in milliseconds). The total number of counts in a feature on one of the rate maps can be found by adding the product of exposure time and counting rate for all pixels in the feature. This is useful for determining the statistical significance of small low-contrast features. Exposure time in other bands will differ somewhat from the C band exposure due to variations in the atmospheric transmission, and because significant amounts of data were included for higher energies which had to be discarded for the C band due to low energy contamination.

TABLE 1

DISCRETE SOURCES REMOVED FROM DATA

B and C Bands	M_1, M_2, I, J, 2-6 keV Bands
Cygnus Loop	Cygnus Loop
Vela-Puppis Supernova Remnants	Vela-Puppis Supernova Remnants
HZ 43, AM Her, Sco X-1	All 4U Catalog[a] sources brighter than 20 Uhuru cts s^{-1} (67 sources)
U Gem	

[a]Forman et al. (1978).

TABLE 2

RESIDUAL DISCRETE SOURCES

Approximate Location of Feature (ℓ, b)	Appears in Bands	Contributing Sources
330°, +17°	C, M_1, M_2, I, J	Lupus Loop, SN1006
210°, -18°	I, J, 2-6	Orion Trapezium Sources
284°, +75°	J, 2-6	Virgo Cluster (4U1228+12)
120°, + 0°	J, 2-6	Several weak 4U[a] sources
315°, +30°	2-6	Several weak 4U sources
20°, + 0°	I, J, 2-6	May be due to sources seen[b] on OSO-7, SAS-3, Ariel-5, and HEAO-1
275°, - 5°	2-6	
315°, + 0°	I, J, 2-6	

[a]Forman et al. (1978).

[b]Amnuel et al. (1982).

TABLE 3

BAND CHARACTERISTICS AND RESPONSE TO SIMPLE SPECTRA

	(Units)	B	C	M_1	M_2	I	J	2-6
E_{eff}[a] for $E^{-1.5}$ photon spectrum	(keV)	0.169	0.225	0.638	0.812	1.06	1.59	3.49
E_{eff} for $E^{-2.5}$ photon spectrum	(keV)	0.157	0.214	0.611	0.786	1.02	1.52	3.11
$\int A*\Omega\ dE$	(cm^2 sr keV)	0.117	0.54	0.42	1.14	3.54	11.7	55.
Ω (Sclid Angle)	(sr)	0.0163	0.0193	0.0132	0.0132	0.0132	0.0132	0.0132
All-Sky Average Counting Rate	(cts s^{-1})	49	133	25	39	57	74	103
Response to:	(all cts s^{-1})							
10^{-8} ergs cm^{-2} s^{-1} sr^{-1} keV^{-1} (E^{-1} photon spectrum)[b]		4.1	14.5	4.0	8.6	20.7	45.	93.
10^{-8} ergs cm^{-2} s^{-1} sr^{-1} keV^{-1} at E_{eff} ($E^{-2.5}$ photon spectrum)[b]		4.0	14.2	3.9	8.5	20.4	44.	89.
1.0 $E^{-1.5}$ photons cm^{-2} s^{-1} sr^{-1} keV^{-1}		1.62	4.93	0.80	1.54	3.23	5.69	8.12
1.0 E^{-2} photons cm^{-2} s^{-1} sr^{-1} keV^{-1} (= 0.035 U.F.U. deg^{-2})		4.06	10.6	1.02	1.73	3.19	4.59	4.54
1.0 $E^{-2.5}$ photons cm^{-2} s^{-1} sr^{-1} keV^{-1}		10.3	23.0	1.31	1.96	3.17	3.74	2.61
11 $E^{-1.4}$ photons cm^{-2} s^{-1} sr^{-1} keV^{-1}, $N_H = 0$		14.9	46.6	8.41	16.6	35.7	65.4	101.
11 $E^{-1.4}$ photons cm^{-2} s^{-1} sr^{-1} keV^{-1}, $N_H = 2x10^{20}$ cm^{-2}		1.5	15.3	7.5	15.4	34.3	64.4	100.
Peak response to 1 U.F.U. point source[c]		2.33	5.26	0.74	1.28	2.37	3.47	3.37

[a] E_{eff} is mean energy of detected photons in band.

[b] Note that counting rates in a band can be converted to differential energy fluxes at the effective energy for that band with very little sensitivity to the assumed spectral form.

[c] Unabsorbed E^{-2} spectrum assumed. See §IIIe for discussion of appearance of point sources on maps.

TABLE 4

FLIGHT PARAMETERS

Flight	Date	Time	Place[a]	Peak Altitude (km)	Zenith ℓ	Zenith b	Solar Zenith Angle	K_p[b]	Payload[c]
13.083	1972 December 8	$06^h\ 26^m\ 02^s$ UT	White Sands	184.	168°2	-9°5	168°4	1+	III
13.103	1973 November 1	$15^h\ 30^m\ 00^s$ UT	Woomera	174.	227°9	-56°4	134°1	1-	IV
13.102	1973 November 12	$14^h\ 00^m\ 00^s$ UT	Woomera	178.	226°8	-66°6	130°2	2	III
13.084	1974 July 20	$06^h\ 10^m\ 01^s$ UT	White Sands	196.	64°2	+12°8	125°1	3-	IV
13.049	1975 November 8	$05^h\ 20^m\ 00^s$ UT	White Sands	179.	131°8	-29°2	154°7	2	IV
13.122	1977 January 15	$06^h\ 17^m\ 01^s$ UT	White Sands	196.	183°5	+15°3	163°1	4	IV
26.061	1977 May 25	$07^h\ 25^m\ 00^s$ UT	White Sands	192.	54°0	+41°6	125°8	1+	IV
13.137	1978 May 6	$06^h\ 55^m\ 01^s$ UT	White Sands	200.	52°2	+63°7	130°7	1	IV
25.045	1979 March 15	$05^h\ 20^m\ 00^s$ UT	White Sands	216.	193°7	+50°7	140°0	1+	IV
25.051	1980 January 21	$08^h\ 05^m\ 00^s$ UT	White Sands	216.	192°1	+41°4	162°7	1	IV

[a]White Sands: 106°4 W, 32°8 N.
Woomera: 136°5 E, 30°9 S.

[b]Magnetic disturbance index, K_p, at time of launch.

[c]See text.

TABLE 5

ENERGY BAND DEFINITIONS

Energy Band	Pulse Height Limits (keV)	20% response points (keV)
B	0.06 - 0.35	0.13 - 0.188
C	0.06 - 0.45	0.16 - 0.284
M_1	0.50 - 0.65	0.44 - 0.93
M_2	0.65 - 0.85	0.60 - 1.1
I	0.85 - 1.2	0.77 - 1.5
J	1.2 - 2.0	1.1 - 2.2
2-6	2.0 - 6.0	1.8 - 6.3

REFERENCES

Amnuel, P. R., Guseinov, O. H., and Rakhamimov, Sh. Yu. 1982, Ap. Space Sci., 82, 3.

Axford, W. I. 1972, NASA Pub. No. SP-308 (Asilomar Solar Wind Conference), p. 609.

Berkhuijsen, E. M., Haslam, C. G. T., and Salter, C. J. 1971, Astr. Ap., 14, 252.

Bohlin, R. C., Savage, B. D., and Drake, J. F. 1978, Ap. J., 224, 132.

Boldt, E. 1981, Comments on Astrophysics, 9, 97.

Borken, R. J., and Iwan, D. C. 1977, Ap. J., 218, 511.

Bowyer, C. S., and Field, G. B. 1969, Nature, 223, 573.

Bregman, J. N. 1982, Nature, 298, 10.

Brown, R. L., and Gould, R. J. 1970, Phys. Rev. D, 1, 2252.

Bruhweiler, F. C., and Kondo, Y. 1982, Ap. J., 259, 232.

Bunner, A. N. 1978, Ap. J., 220, 261.

Bunner, A. N., Coleman, P. L., Kraushaar, W. L., McCammon, D., Palmieri, T. M., Shilepsky, A., and Ulmer, M. 1969, Nature, 223, 1222.

Bunner, A. N., Sanders, W. T., and Nousek, J. A. 1979, Ap. J. (Letters), 228, L29.

Burrows, D. N. 1982, Ph.D. thesis, University of Wisconsin, Madison.

Burstein, P. H. 1976, Ph.D. thesis, University of Wisconsin, Madison.

Burstein, P., Borken, R. J., Kraushaar, W. L., and Sanders, W. T. 1977, Ap. J., 213, 405.

Cash, W., Bowyer, S., and Lampton, M. 1979, Astr. Ap., 80, 67.

Cash, W., Charles, P., Bowyer, S., Walter, F., Garmire, G., and Riegler, G. 1980, Ap. J. (Letters), 238, L71.

Chevalier, R. A., and Oegerle, W. R. 1979, Ap. J., 227, 398.

Clark, B. G. 1965, Ap. J., 142, 1398.

Cleary, M. N., Heiles, C., and Haslam, C. G. T. 1979, Astr. Ap. Suppl., 36, 95.

Davelaar, J., Bleeker, J. A. M., and Deerenberg, A. J. M. 1980 Astr. Ap., 92, 231.

Davidsen, A., Shulman, S., Fritz, G., Meekins, J. F., Henry, R. C., and Friedman, H. 1972, Ap. J., 177, 629.

Dickey, J. M. 1977, Ph.D. thesis, Cornell University.

———. 1979, Ap. J., 233, 558.

Dickey, J. M., Salpeter, E. E., and Terzian, Y. 1979, Ap. J., 228, 465.

Dickey, J. M., and Terzian, Y. 1978, Astr. Ap., 70, 415.

Forman, W., Jones, C., Cominsky, L., Julien, P., Murray, S., Peters, G., Tananbaum, H., and Giacconi, R. 1978, Ap. J. Suppl., 38, 357.

Fried, P. M., Nousek, J. A., Sanders, W. T., and Kraushaar, W. L. 1980, Ap. J., 242, 987.

Grader, R. J., Hill, R. W., Seward, F. D., and Hiltner, W. A. 1970, Ap. J., 159, 201.

Greisen, E. W. 1976, Ap. J., 203, 371.

Hayakawa, S., Iwanami, H., Kunieda, H., Nagase, F., and Yamashita, K. 1979a, in X-ray Astronomy, ed. W. A. Baity and L. E. Peterson (Oxford: Pergammon).

Hayakawa, S., Kato, T., Makino, F., Ogawa, H., and Tanaka, Y. 1971, Rept. Ionos. and Space Res. Japan, 25, 1.

Hayakawa, S., Kato, T., Makino, F., Ogawa, H., Tanaka, Y., Yamashita, K., Matsuoka, M., Miyamoto, S., Oda, M., and Ogawara, Y. 1970, in Non-Solar X- and Gamma-Ray Astronomy, ed. L. Gratton (Dordrecht: Reidel), p. 121.

Hayakawa, S., Kato, T., Nagase, F., and Yamashita, K. 1979b, Publ. Ast. Soc. Japan, 31, 71.

Heiles, C. 1974, Astr. Ap. Suppl., 14, 557.

Heiles, C., Chu, Y., Reynolds, R. J., Yegingil, I., and Troland, T. H. 1980, Ap. J., 242, 533.

Heiles, C., Stark, A. A., and Kulkarni, S. 1981, Ap. J. (Letters), 247, L73.

Henke, B. L., Elgin, R. L., Lent, R. E., and Ledingham, R. B. 1967, Norelco Reporter, XIV, 112.

Iwan, D., Marshall, F. E., Boldt, E. A., Mushotzky, R. F., Shafer, R. A., and Stottlemyer, A. 1982, Ap. J., 260, 111.

Iwan, D. C. 1978, Ph.D. thesis, University of Wisconsin, Madison.

———. 1980, Ap. J., 239, 316.

Jacchia, L. G. 1972, in Cospar International Reference Atmosphere 1972, compiled by The Committee for the COSPAR International Reference Atmosphere (CIRA) of COSPAR Working Group 4 (Berlin: Akademie-Verlag), p. 227.

Jenkins, E. B. 1978a, Ap. J., 219, 845.

———. 1978b, Ap. J., 220, 107.

Jenkins, E. B., and Meloy, D. A. 1974, Ap. J. (Letters), 193, L121.

Kraushaar, W. L. 1974, in Proceedings of the Workshop on Electron Contamination in X-Ray Astronomy Experiments, ed. S. Holt (GSFC).

Levine, A., Rappaport, S., Halpern, J., and Walter, F. 1977, Ap. J., 211, 215.

Long, K. S., Agrawal, P. C., and Garmire, G. P. 1976, Ap. J., 206, 411.

Luhmann, J. G., Rugge, H. R., Blake, J. B., and Christopher, L. A. 1979, Geophys. Res. Lett., 6, 25.

Marshall, F. E., Boldt, E. A., Holt, S. S., Miller, R. B., Mushotzky, R. F., Rose, L. A., Rothschild, R. E., and Serlemitsos, P. J. 1980, Ap. J., 235, 4.

Marshall, F. J. 1981, Bull. Am. Astr. Soc., 13, 788.

———. 1982a, private communication.

———. 1982b, Ph.D. thesis, Massachusetts Institute of Technology.

McCammon, D. 1971, Ph.D. thesis, University of Wisconsin, Madison.

McCammon, D., Bunner, A. N., Coleman, P. L., and Kraushaar, W. L. 1971, Ap. J. (Letters), 168, L33.

McCammon, D., Meyer, S. S., Sanders, W. T., and Williamson, F. O. 1976, Ap. J., 209, 46.

McKee, C. F., and Ostriker, J. P. 1977, Ap. J., 218, 148.

Morrison, J. P. 1979, Ph.D. thesis, University of Wisconsin, Madison.

Naranan, S., Shulman, S., Friedman, H., and Fritz, G. 1976, Ap. J., 208, 718.

Nousek, J. A., Fried, P. M., Sanders, W. T., and Kraushaar, W. L. 1982, Ap. J., 258, 83.

Payne, H. E., Salpeter, E. E., and Terzian, Y. 1982, Ap. J. Suppl., 48, 199.

Radhakrishnan, V. 1974, in IAU Symposium 60, Galactic Radio Astronomy, ed. F. J. Kerr and S. C. Simonson, III (Dordrecht: Reidel), p. 3.

Raymond, J. C., and Smith, B. W. 1977, Ap. J. Suppl., 35, 419.

———. 1979, private communication (update to Raymond and Smith (1977)).

Reynolds, R. J., and Ogden, P. M. 1979, Ap. J., 229, 942.

Ride, S. K., and Walker, A. B. C. Jr. 1977, Astr. Ap., 61, 347.

Rosner, R., Avni, Y., Bookbinder, J., Giaconni, R., Golub, L., Harnden, F. R. Jr., Maxson, C. W., Topka, K., and Vaiana, G. S. 1981, Ap. J. (Letters), 249, L5.

Ryter, C., Cesarsky, C. J., and Audouze, J. 1975, Ap. J., 198, 103.

Sanders, W. T., Burrows, D. N., Kraushaar, W. L., and McCammon, D. 1982, in IAU Symposium No. 101, Supernova Remnants and their X-ray Emission, ed. J. Danziger and P. Gorenstein (Dordrecht: Reidel).

Sanders, W. T., Kraushaar, W. L., Nousek, J. A., and Fried, P. M. 1977, Ap. J. (Letters), 217, L87.

Savage, B. D., and de Boer, K. S. 1981, Ap. J., 243, 460.

Schwartz, D. A. 1979, in (COSPAR) X-Ray Astronomy, ed. W. A. Baity and L. E. Peterson (Oxford: Pergamon), p. 453.

Seward, F. D., and Mitchell, M. 1981, Ap. J., 243, 736.

Spitzer, L. 1956, Ap. J., 124, 40.

Stern, R., and Bowyer, S. 1979, Ap. J., 230, 755.

Toor, A., and Seward, F. D. 1974, A. J., 79, 995.

Verschuur, G. L. 1974, Ap. J. Suppl., 27, 65.

Warwick, R. S., Pye, J. P., and Fabian, A. C. 1980, 190, 243.

Williamson, F., and Maxson, C. W. 1975, Rev. Sci. Inst., 46, 50.

Williamson, F. O. 1974, Ph.D. thesis, University of Wisconsin, Madison.

Williamson, F. O., Sanders, W. T., Kraushaar, W. L., McCammon, D., Borken, R., and Bunner, A. N. 1974, Ap. J. (Letters), 193, L133.

Worrall, D. M., Marshall, F. E., Boldt, E. A., and Swank, J. H. 1982, Ap. J., 255, 111.

Yu, G. 1974, Ap. J., 194, 187.

FIGURE CAPTIONS

FIG. 1.--Net area times solid angle band response functions. (a) B, C, M_1 and M_2 bands; (b) I, J, and 2-6 keV bands.

FIG. 2.--Areas of suspected contamination on the B and C band maps only. Maximum contamination rates estimated for each area are given in cts s^{-1} for both bands. Hatched areas indicate features on these maps which are largely due to contamination.

FIG. 3.--B band (130-188 eV) X-ray intensity maps in galactic coordinates. The shading is proportional to counting rate: one vertical shading line in a pixel per 15 cts s^{-1}. The contour interval is 7.5 cts s^{-1}. (a) Aitoff projection centered on $\ell = 0°$.

FIG. 3B.--Same as (a) except 180°-centered Aitoff and polar equal-area projections.

FIG. 4.--Same as Fig. 3 for C band (160-284 eV) X-ray intensity. One shading line in a pixel per 40 cts s^{-1}. Contour interval is 20 cts s^{-1}.

FIG. 5.--Same as Fig. 3 for M_1 band (440-930 eV) X-ray intensity. One shading line = 10 cts s^{-1}. Contour interval = 5 cts s^{-1}.

FIG. 6.--Same as Fig. 3 for M_2 band (600-1100 eV) X-ray intensity. One shading line = 20 cts s^{-1}. Contour interval = 10 cts s^{-1}.

FIG. 7.--Same as Fig. 3 for I band (770-1500 eV) X-ray intensity. One shading line = 20 cts s^{-1}. Contour interval = 10 cts s^{-1}.

FIG. 8.--Same as Fig. 3a for J band (1100-2200 eV) X-ray intensity. One shading line = 30 cts s^{-1}. Contour interval = 15 cts s^{-1}.

FIG. 9.--Same as Fig. 3a for 2-6 keV band (1800-6300 eV) X-ray intensity. One shading line = 40 cts s^{-1}. Contour interval = 20 cts s^{-1}.

FIG. 10.--Neutral hydrogen column density map for -90 km $s^{-1} < v < +70$ km s^{-1} (Cleary, Heiles, and Haslam 1979). One shading line = 1.0 x 10^{20} H I cm^{-2}. Contour levels are 0.5, 1.5, 2.5 ... x 10^{20} H I cm^{-2}.

FIG. 11.--(a)-(e) Counting rate in band per unit emission measure as a function of temperature for radiation from a plasma with solar abundances in thermal equilibrium (Raymond and Smith 1979). Curves are labeled with column densities of intervening interstellar gas in units of 10^{20} H I cm^{-2}. (f) Total Flux (integrated from 10 eV to 5000 eV) per unit emission measure as a function of temperature. This flux can be converted to the standard cooling coefficient in ergs cm^3 s^{-1} by multiplying by $4\pi(3.1 \times 10^{18}\ cm)^{-1}$.

FIG. 12.--Change in correlation coefficient between C band X-ray intensity (C) and H I column density (N_H) as the H I distribution is rotated around the galactic polar axis with respect to the X-ray data. The cross-correlation coefficient is calculated as $(\langle CN_H\rangle-\langle C\rangle\langle N_H\rangle)[(\langle C^2\rangle-\langle C\rangle^2)(\langle N_H^2\rangle-\langle N_H\rangle^2)]^{-1/2}$ using a 1°.8 x 1°.8 grid. The autocorrelations for X-ray intensity and H I column density are shown respectively as dotted and dashed lines (right-hand scale).

FIG. 13.--Scan paths for the rocket flights used in the survey in galactic coordinates. Portions at >90° zenith angle are not shown. Scan rates were generally about 5°.5 s^{-1}. The path for flight 25.045 is shown as a dashed line.

FIG. 14.--Exposure time map for the C band. (Exposure times for other bands differ somewhat.) The shading is proportional to log of the net exposure time per $(1°.8)^2$ pixel, with one vertical line per pixel = 0.5 in $\log_{10}$ (time in milliseconds). The contour interval is 0.25 in the log. A 20-pixel area of the exposure map with four lines in each pixel would have a total exposure of 2.0 s. If this were the area of a feature on the intensity map with an average rate of 120 cts s^{-1}, there would be a total of 240 counts in the feature.

D. N. BURROWS, W. L. KRAUSHAAR, D. MCCAMMON, and W. T. SANDERS:

Department of Physics, University of Wisconsin, Madison, WI 53706

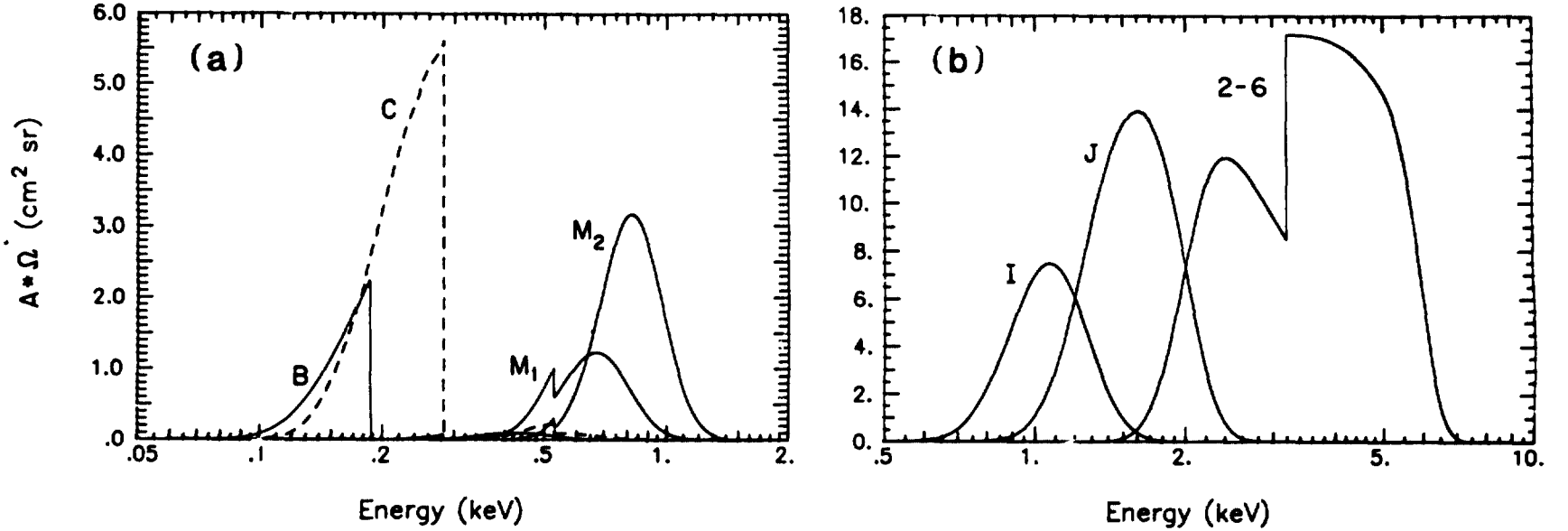

FIG. 1

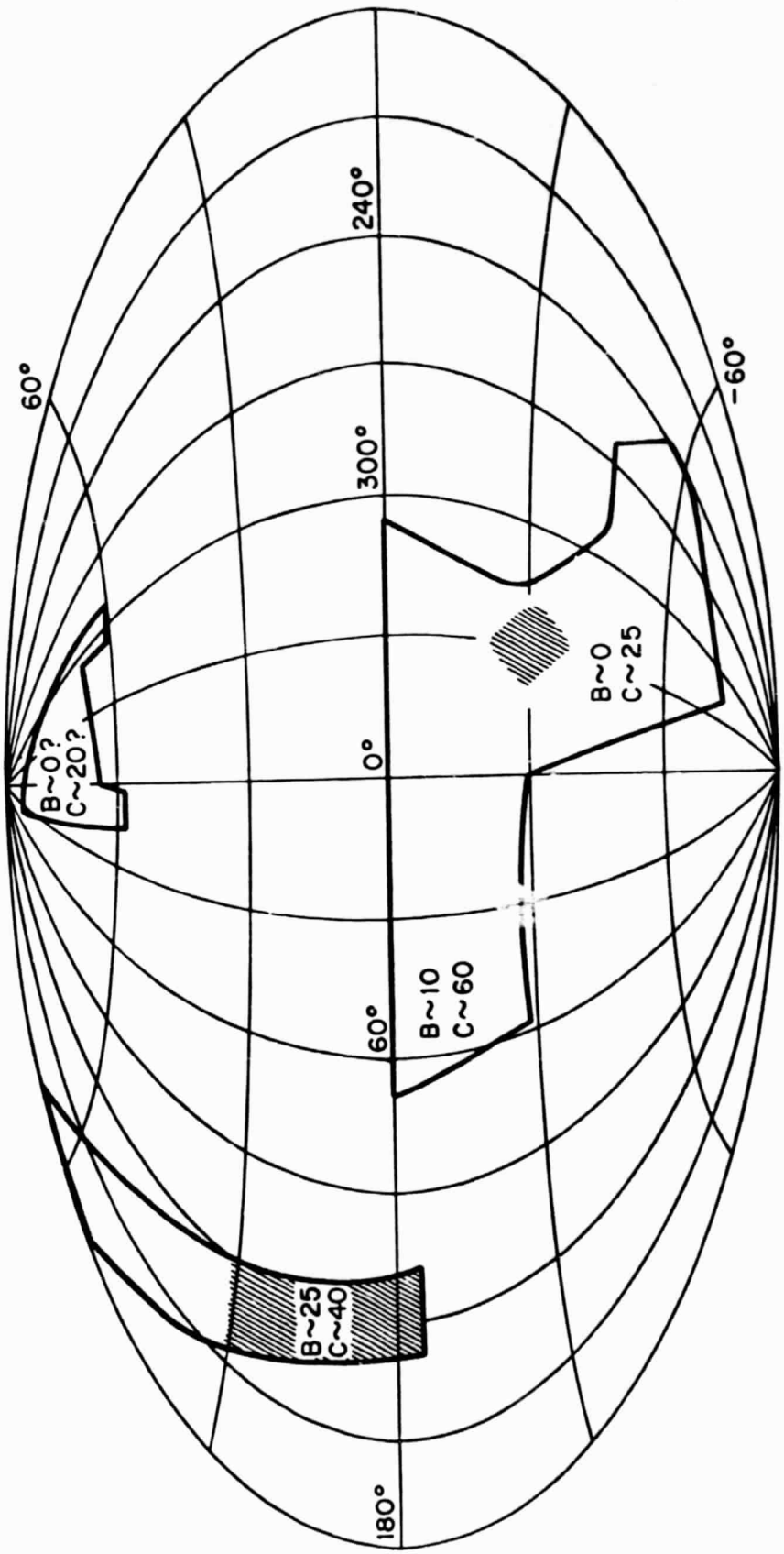

FIG. 2

B Band

FIG. 3

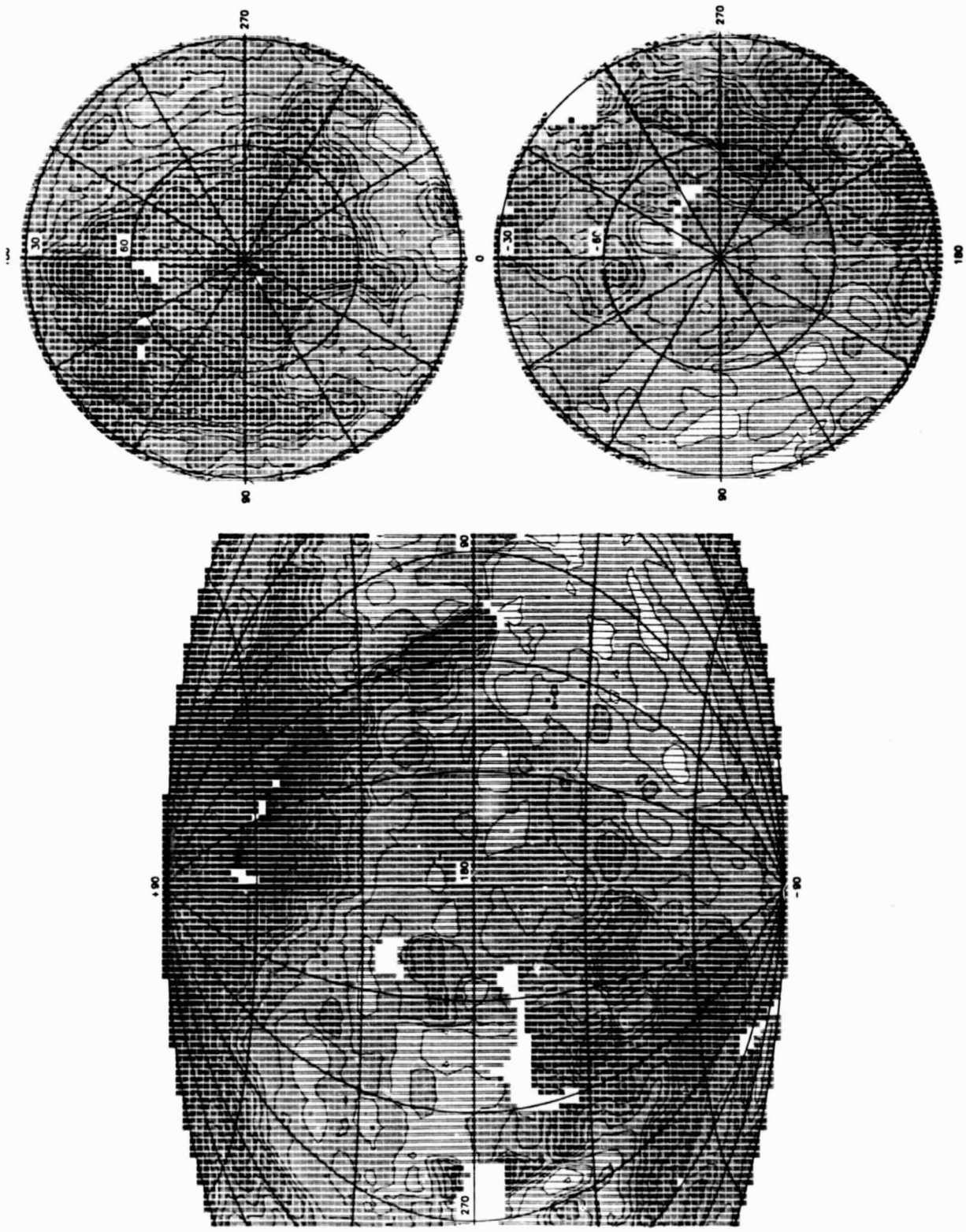

FIG. 3B

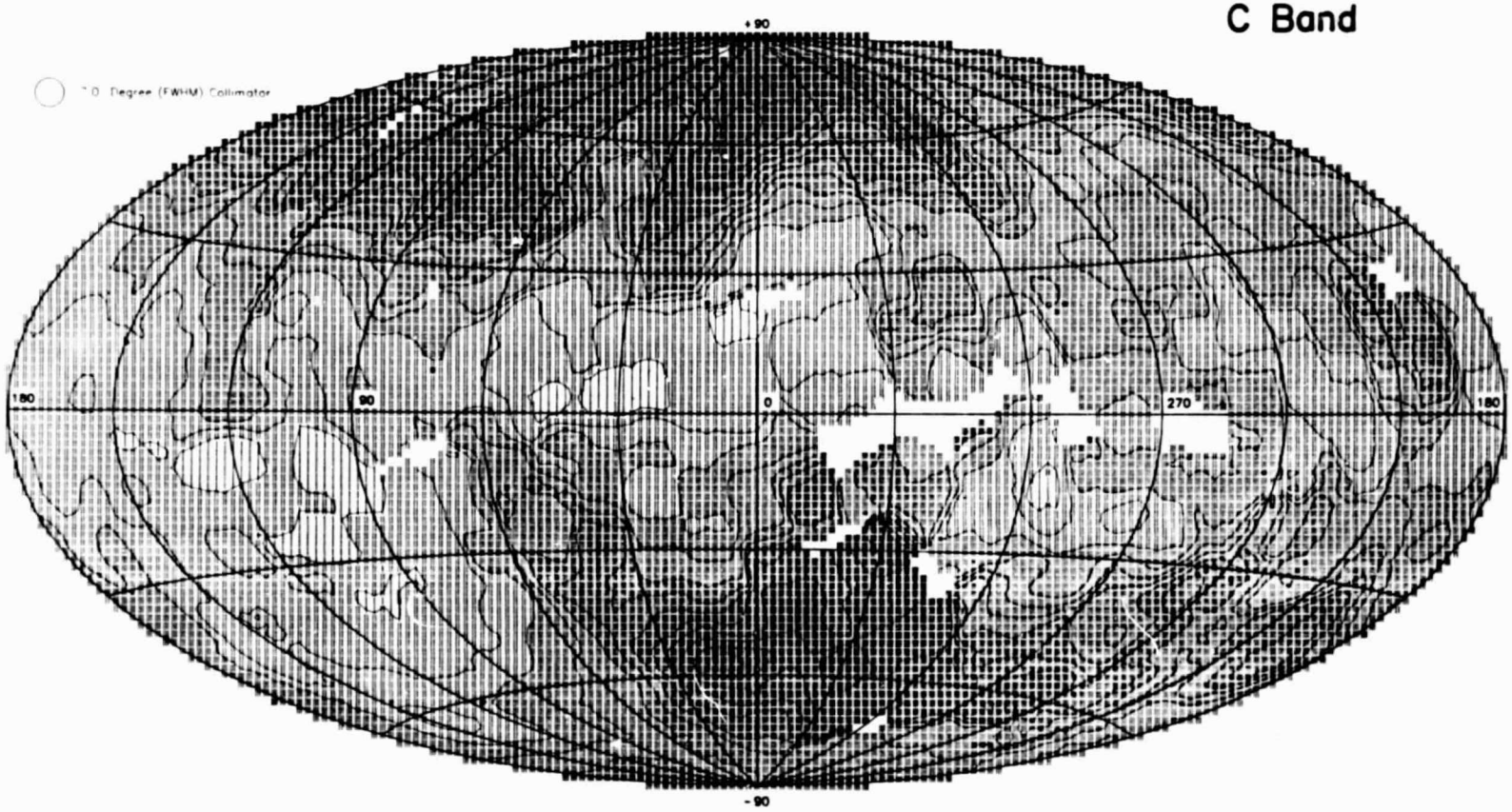

FIG. 4

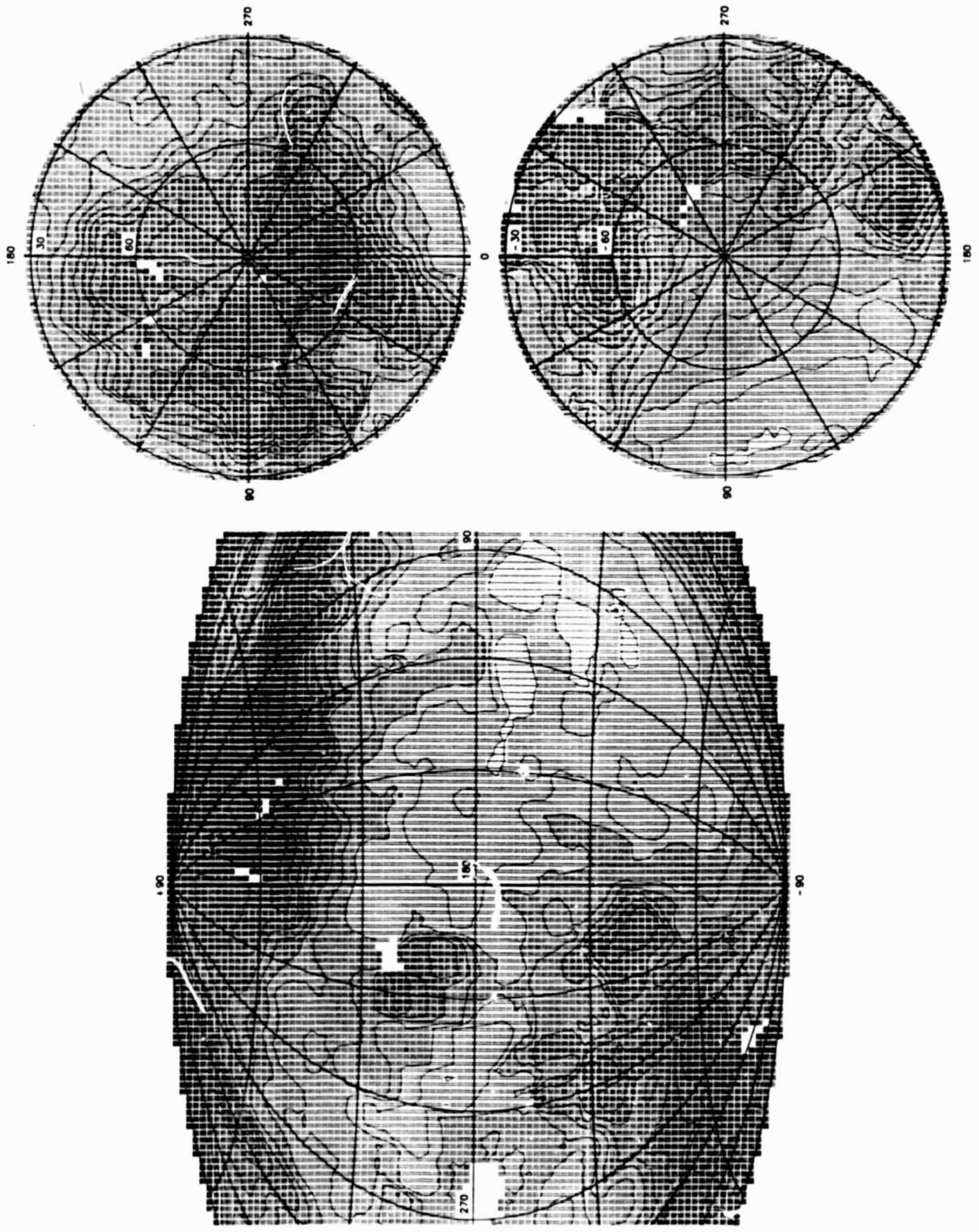

FIG. 4B

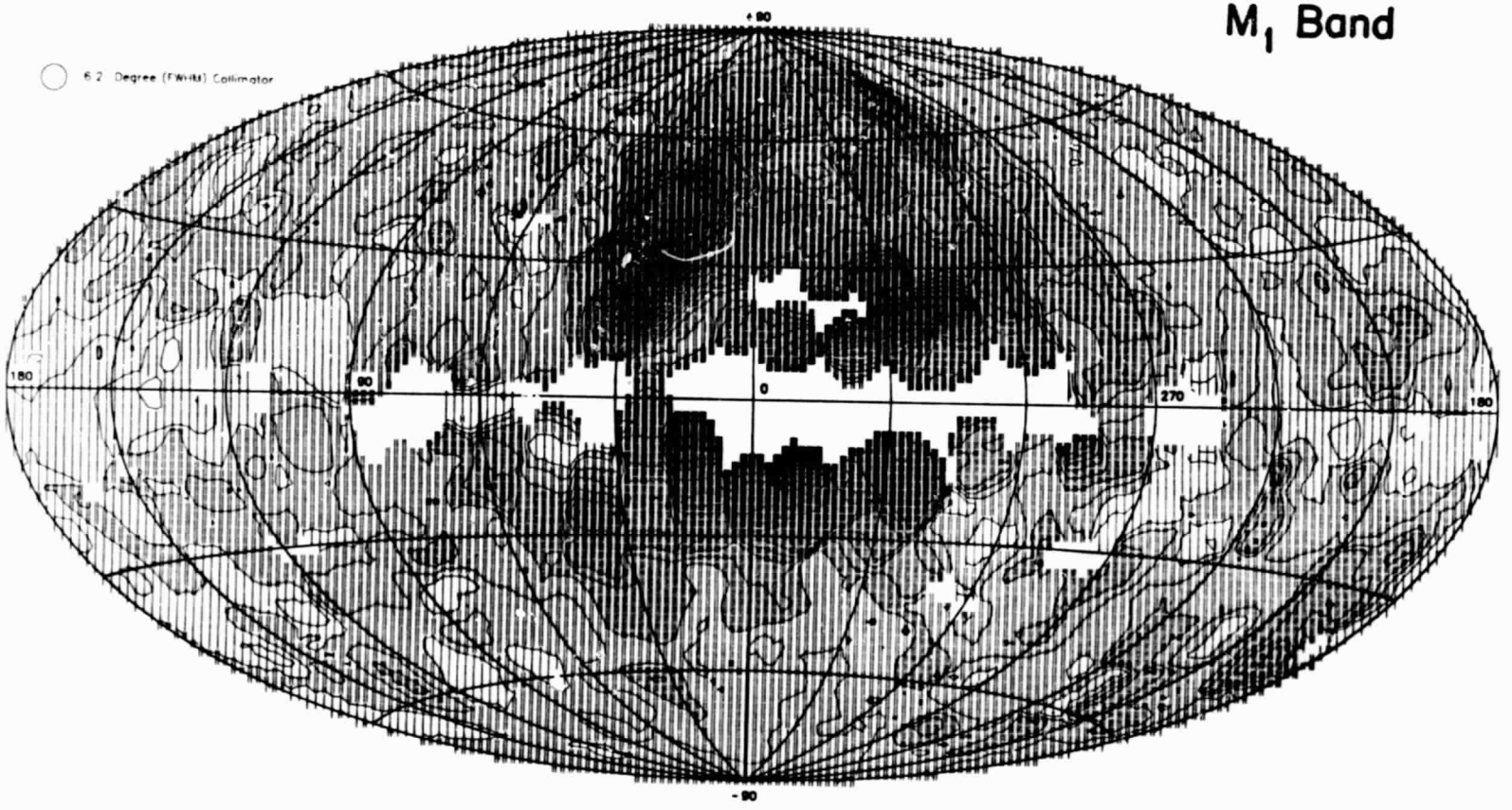

FIG. 5

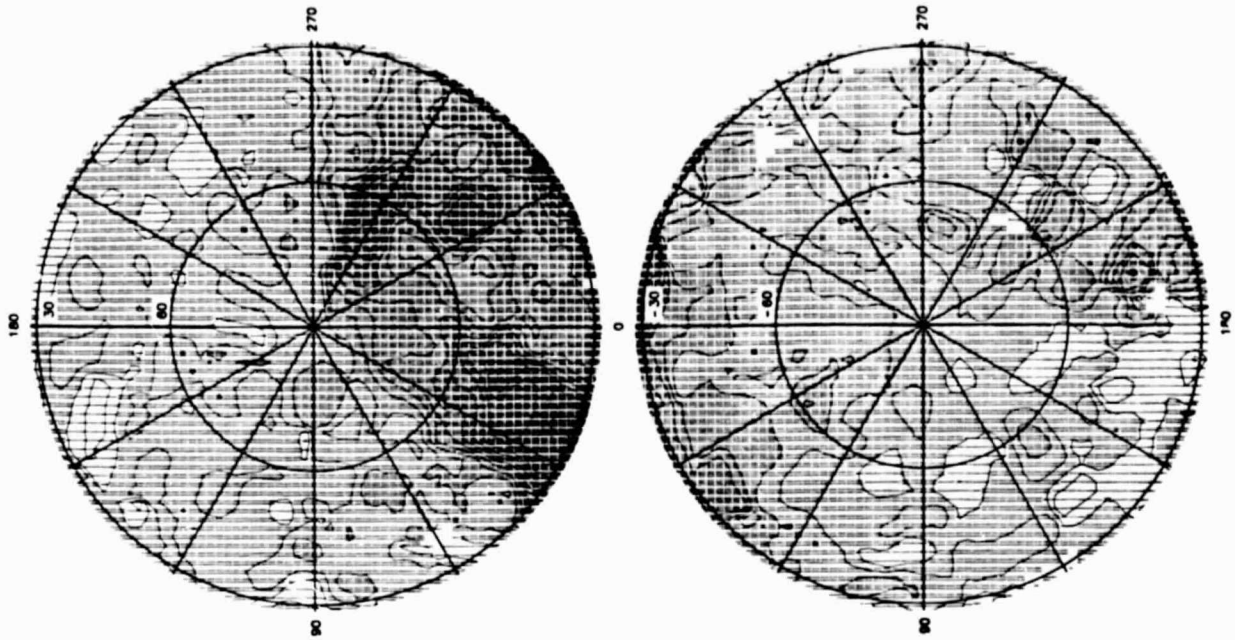

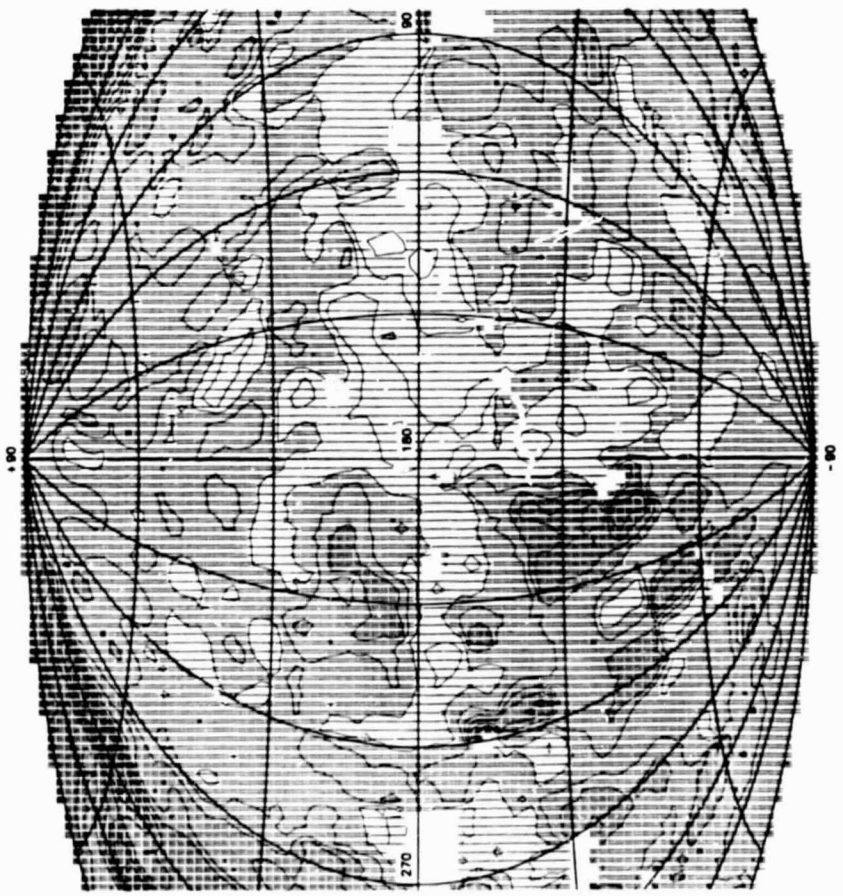

FIG. 5B

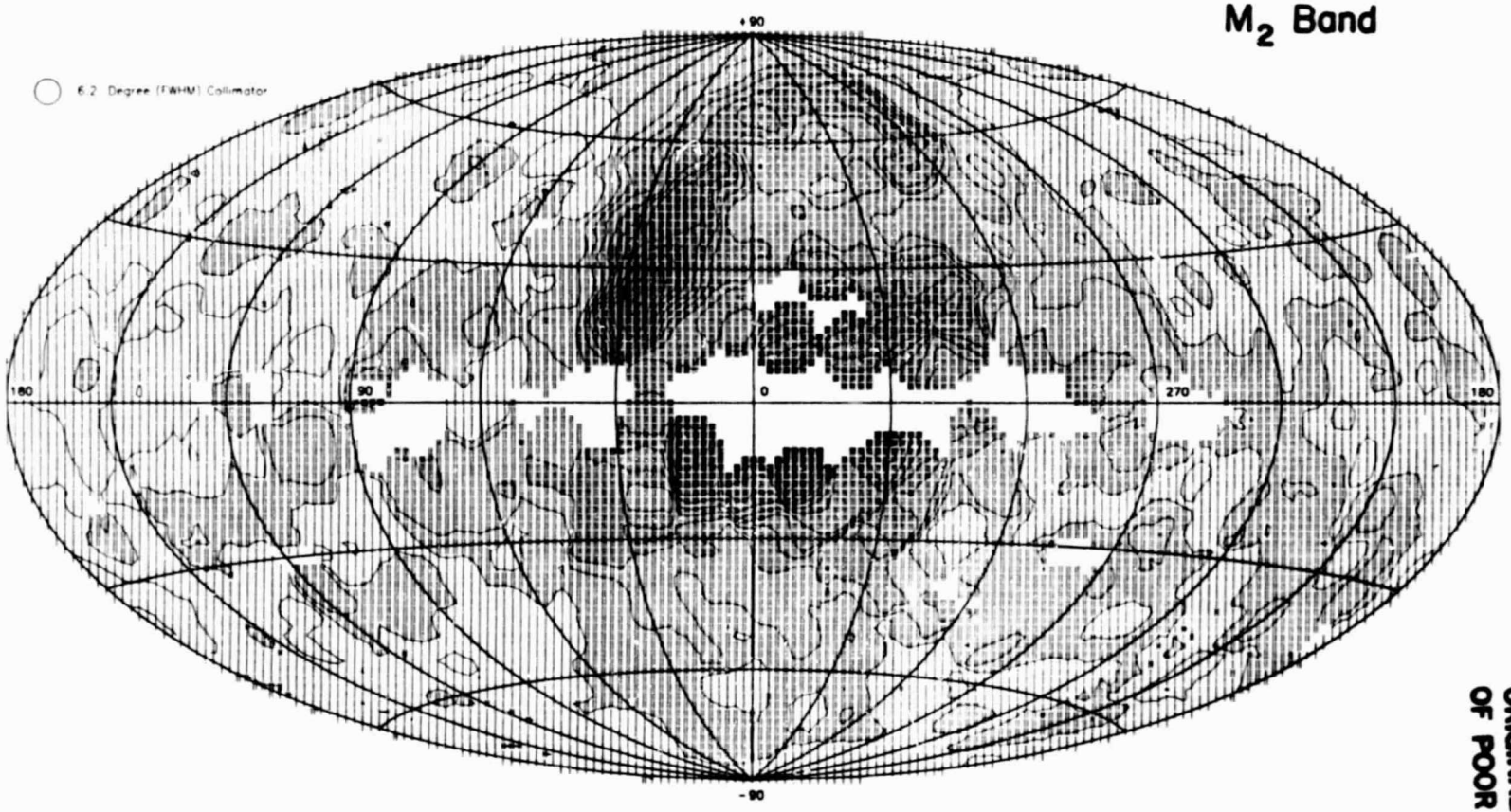

FIG. 6

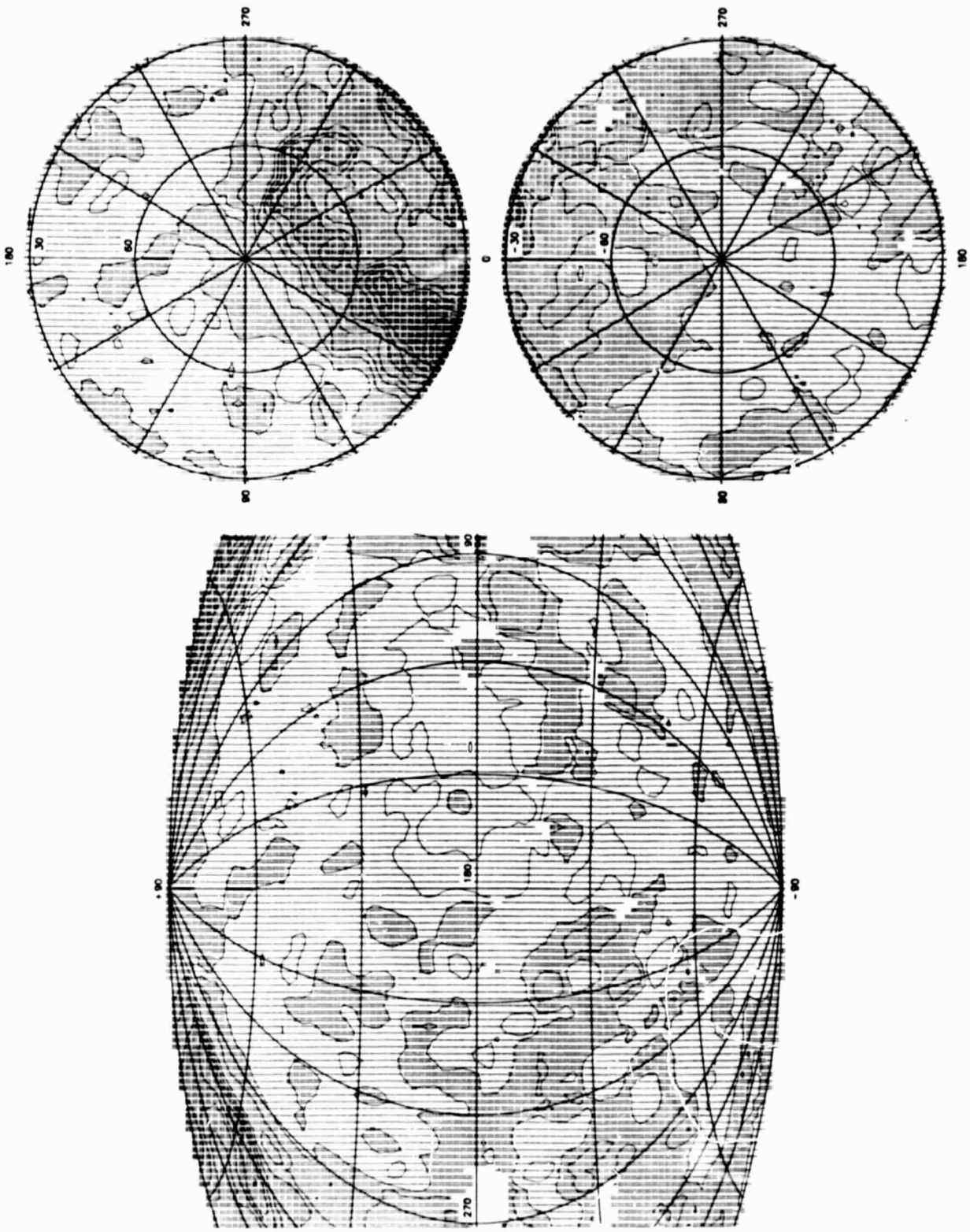

FIG. 6B

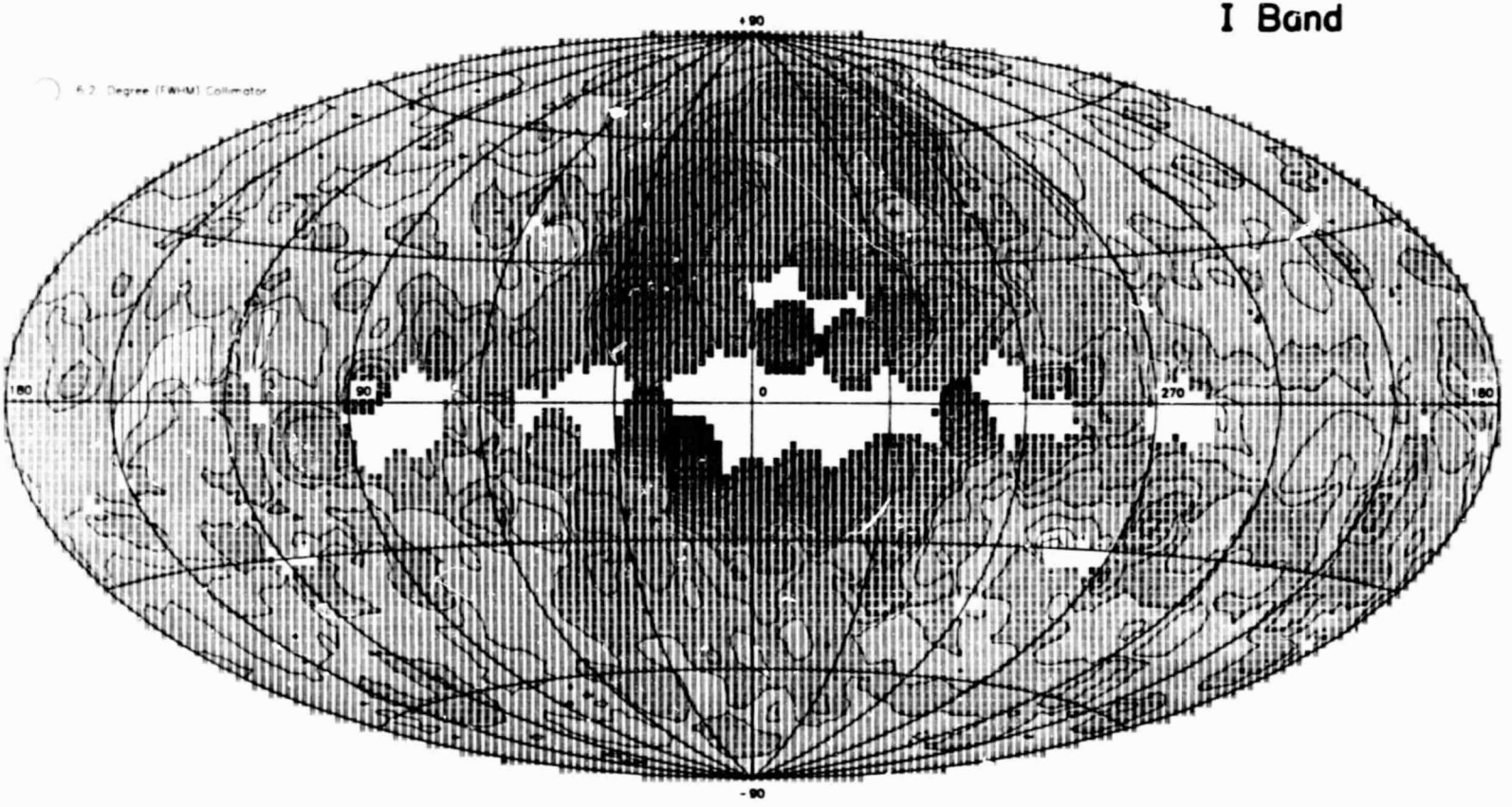

FIG.7

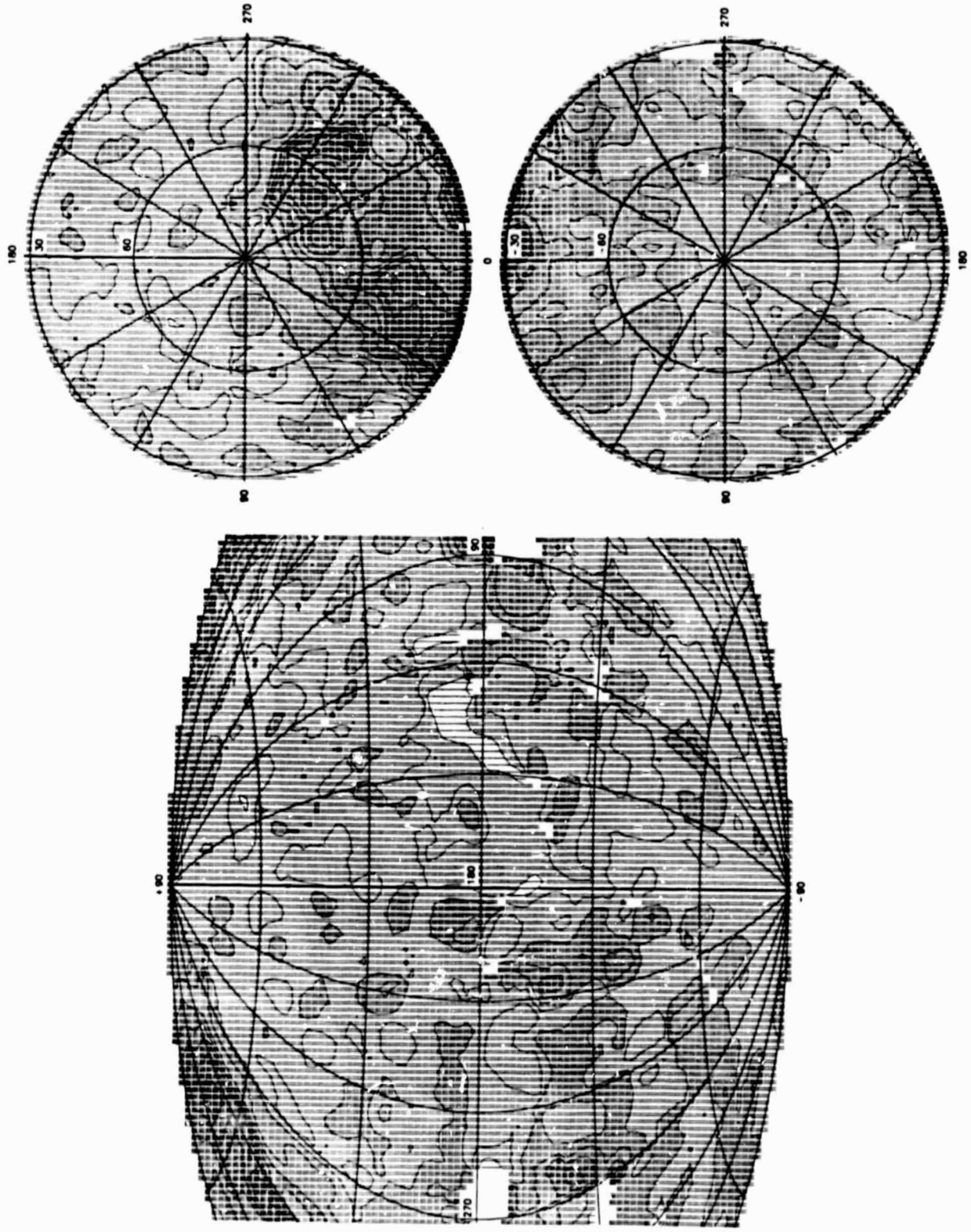

FIG. 7b

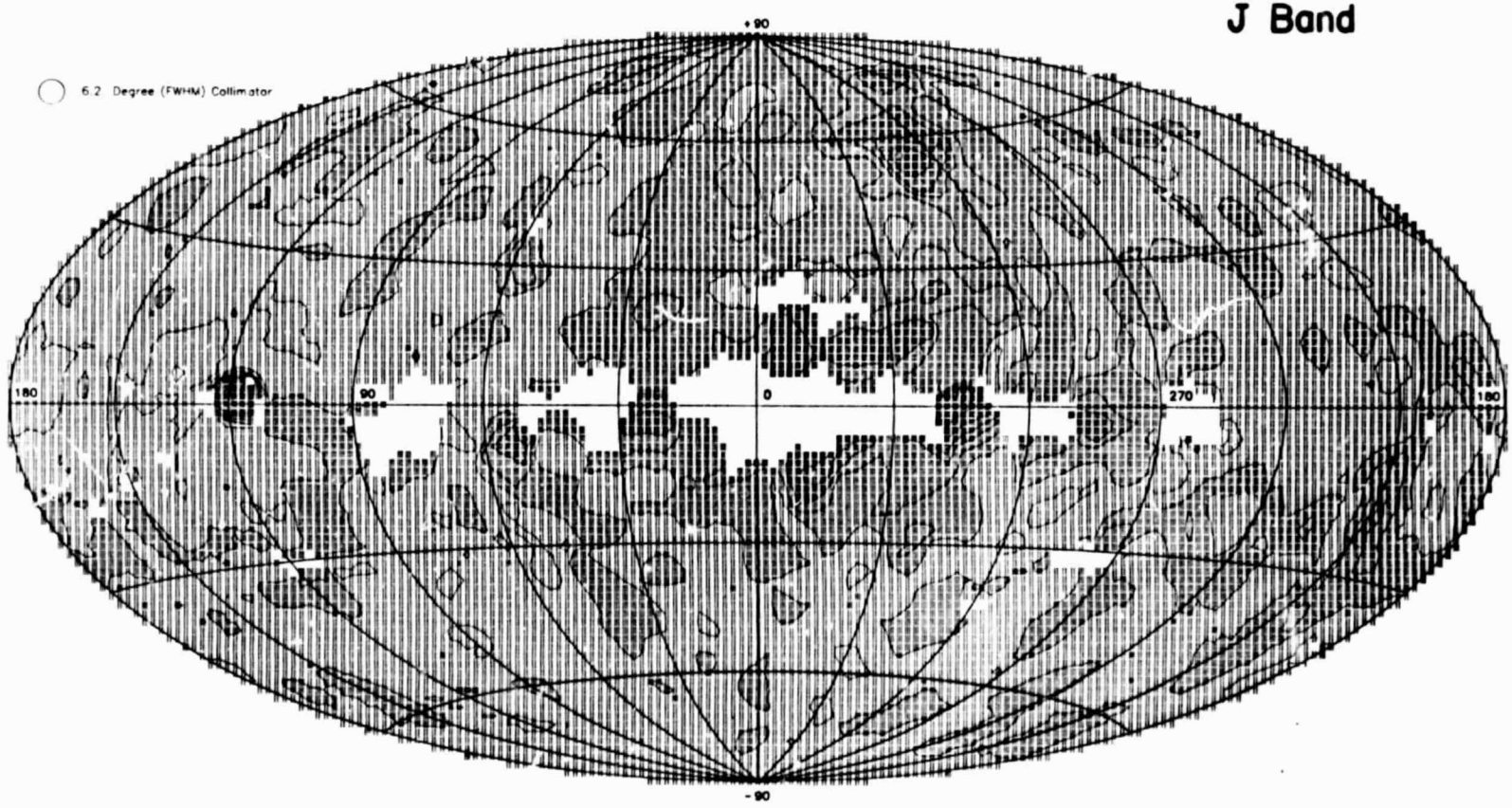

FIG. 8

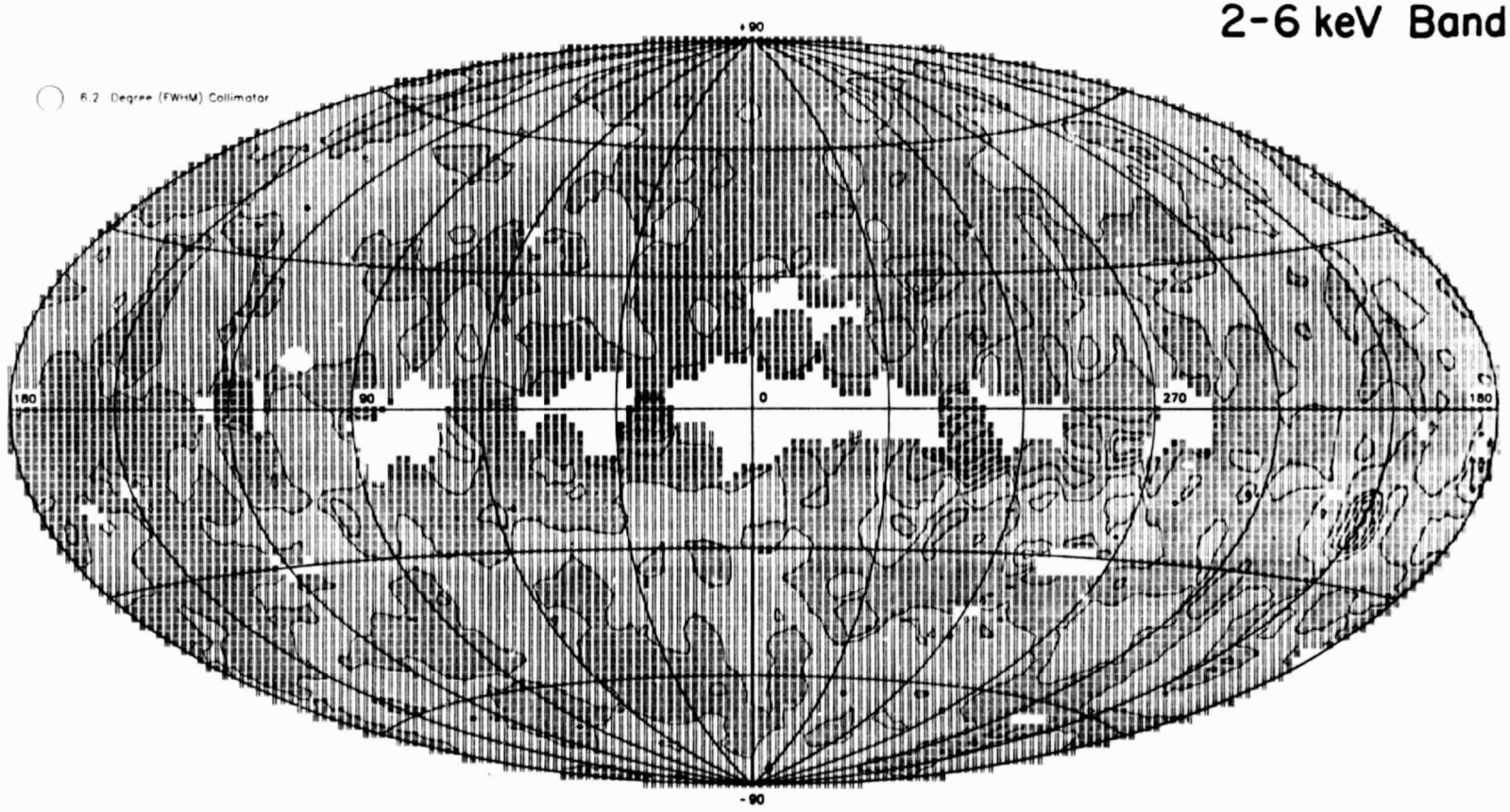

ORIGINAL PAGE IS
OF POOR QUALITY

FIG. 9

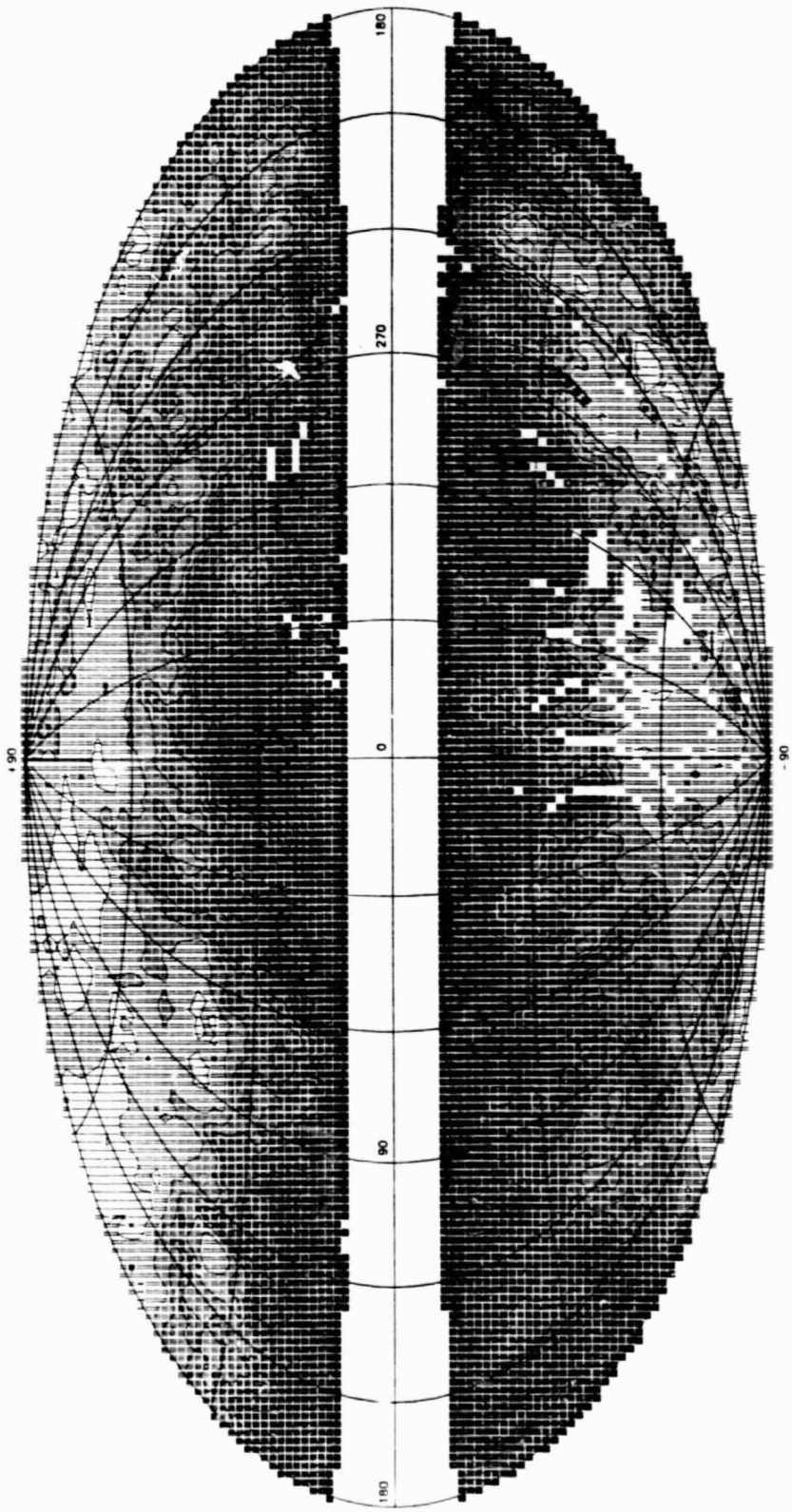

FIG. 10

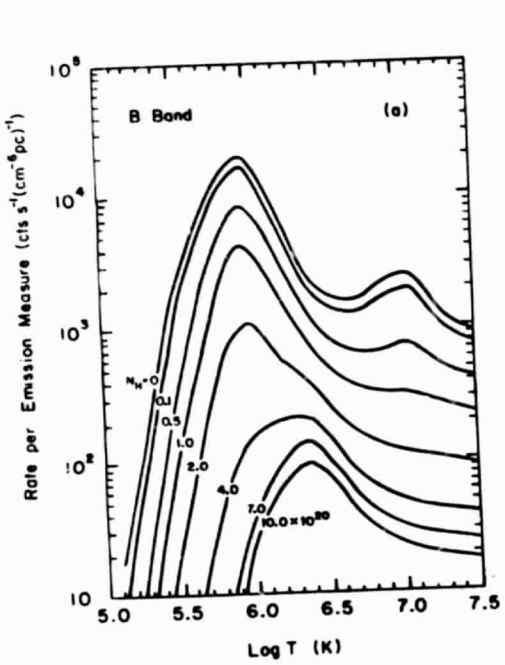

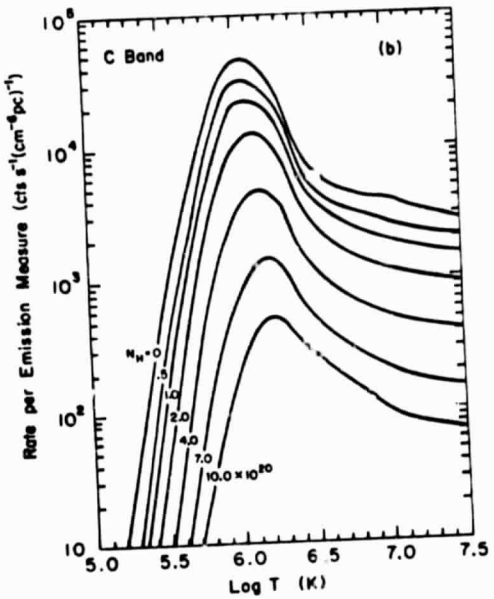

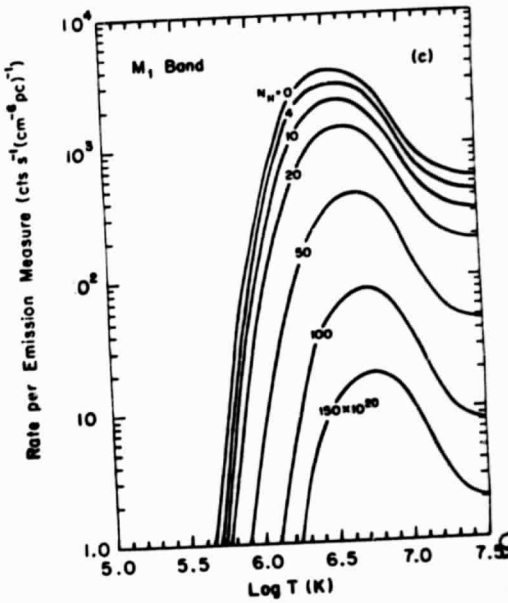

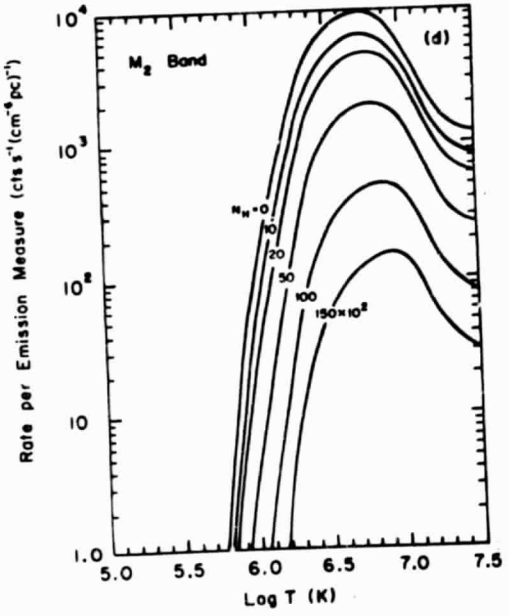

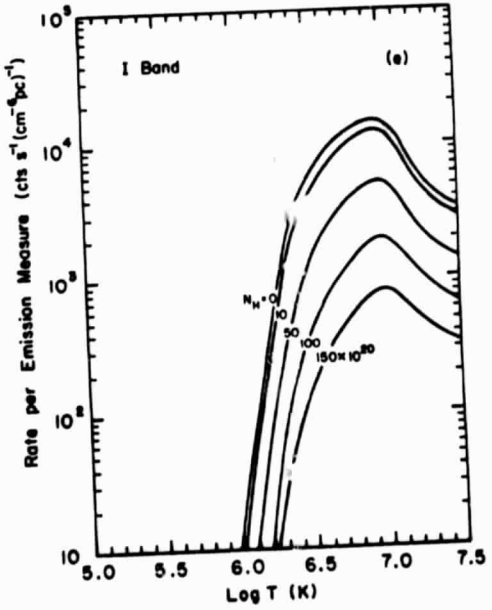

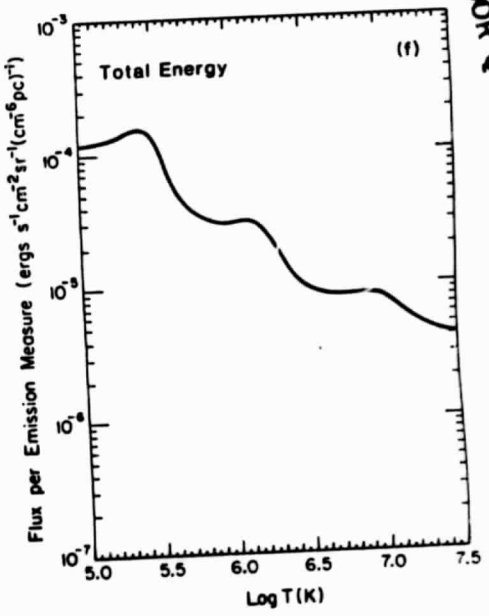

FIG. 11

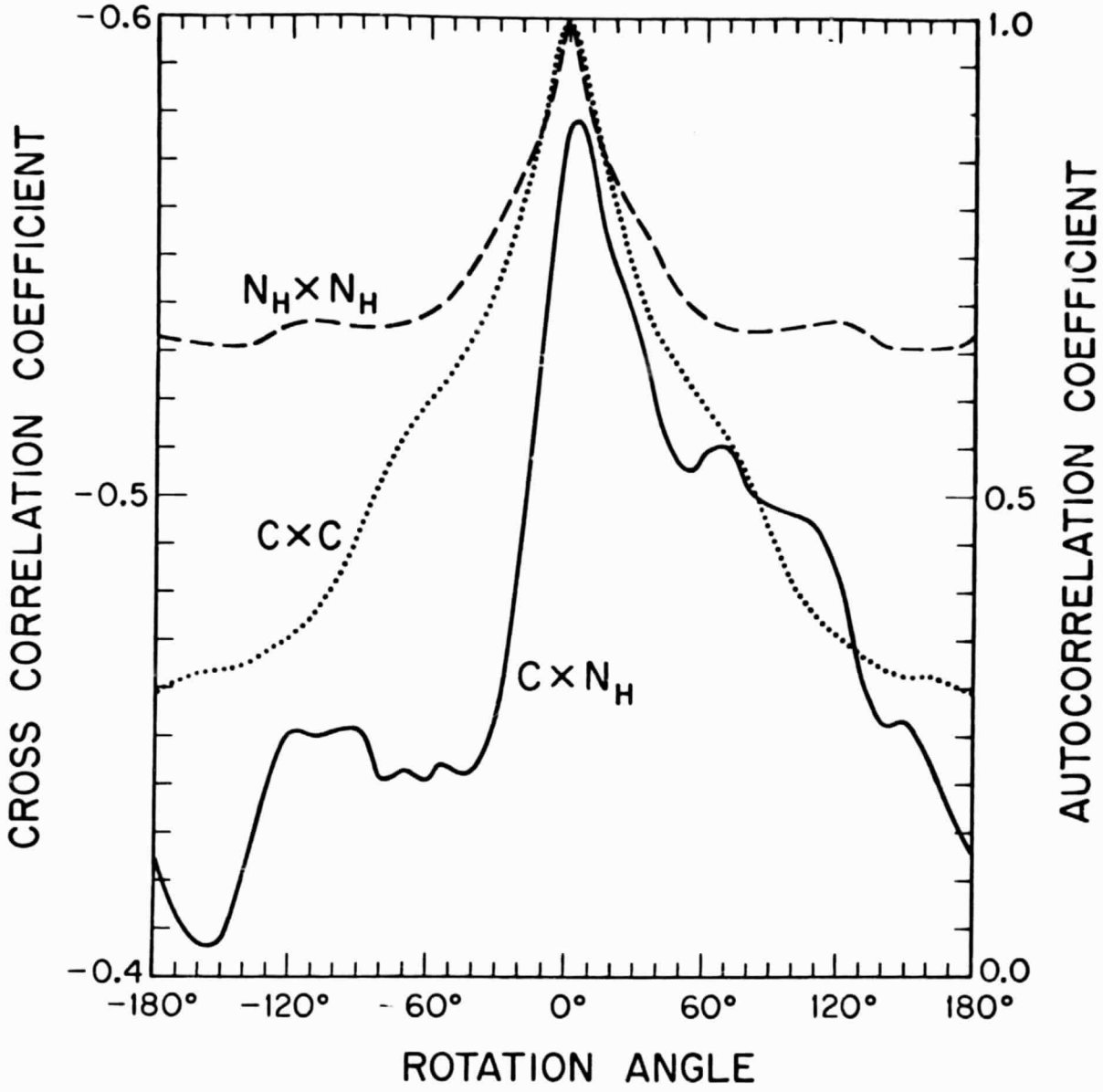

FIG. 12

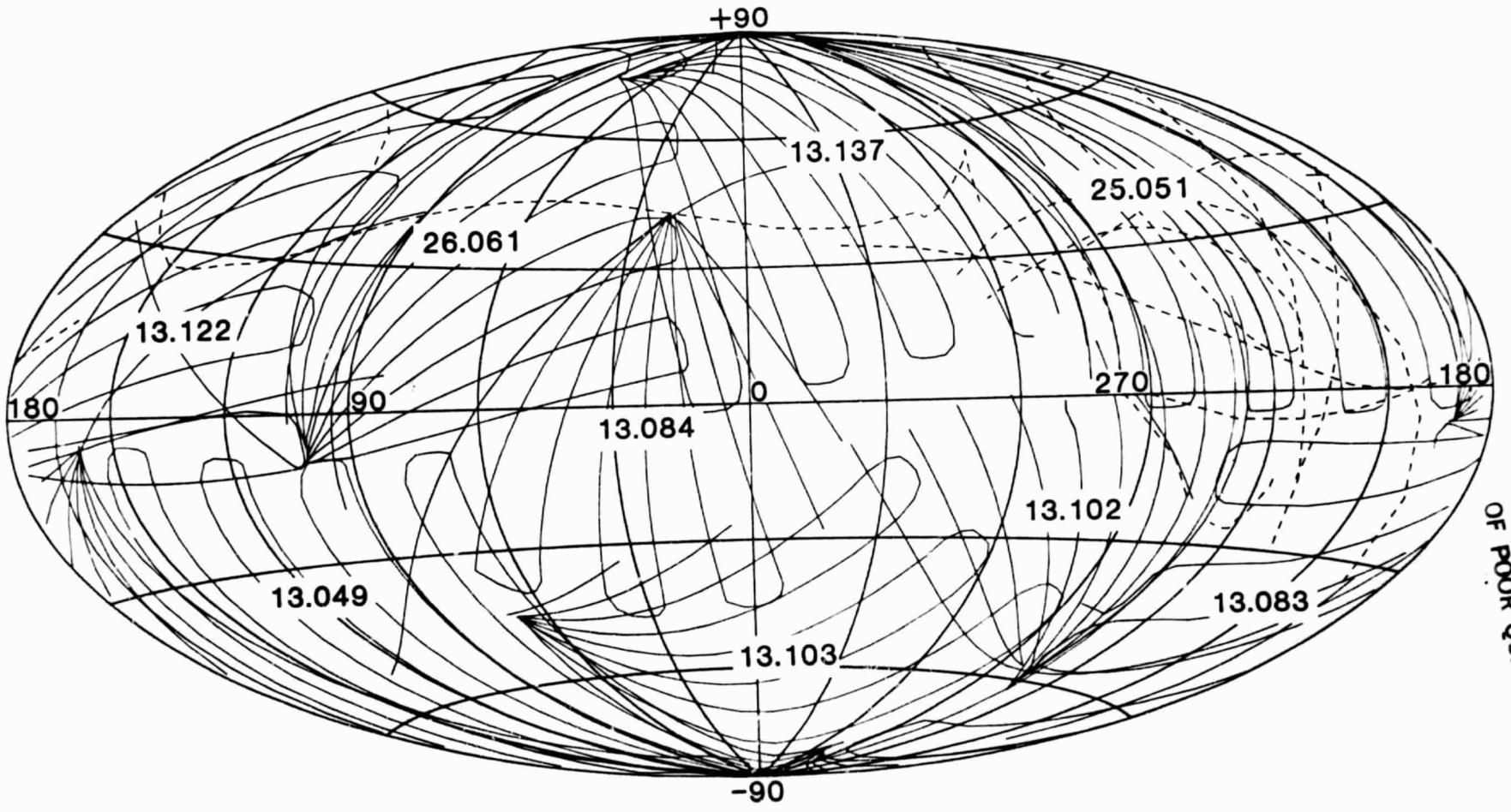

FIG. 13

ORIGINAL PAGE IS
OF POOR QUALITY

FIG. 14